2334 *Inorg. Chem.* **2010**, *49*, 2334–2348
DOI: 10.1021/ic9022272

Inorganic Chemistry
Article

Monometallic and Bimetallic Ruthenium(II) Complexes Derived from 4,5-Bis(benzimidazol-2-yl)imidazole (H_3Imbzim) and 2,2′-Bipyridine as Colorimetric Sensors for Anions: Synthesis, Characterization, and Binding Studies

Debasish Saha,[†] Shyamal Das,[†] Chanchal Bhaumik,[†] Supriya Dutta,[‡] and Sujoy Baitalik*,[†]

[†]*Department of Chemistry, Inorganic Chemistry Section, Jadavpur University, Kolkata 700032, India, and*
[‡]*Department of Inorganic Chemistry, Indian Association for the Cultivation of Science, Kolkata 700 032, India*

Received November 11, 2009

Mixed-ligand monometallic and bimetallic ruthenium(II) complexes of compositions $[(bpy)_2Ru(H_3Imbzim)](ClO_4)_2 \cdot 2H_2O$ (**1**) and $[(bpy)_2Ru(H_2Imbzim)Ru(bpy)_2](ClO_4)_3 \cdot CH_2Cl_2$ (**2**), where H_3Imbzim = 4,5-bis(benzimidazol-2-yl)imidazole and bpy = 2,2′-bipyridine, have been synthesized and characterized using standard analytical and spectroscopic techniques. The X-ray crystal structures of both compounds have been determined and showed that **1** crystallized in the triclinic form with space group $P\bar{1}$ and **2** is in the monoclinic form with space group $P2(1)/m$. The anion binding properties of complexes **1** and **2**, as well as those of the parent H_3Imbzim, were thoroughly investigated in an acetonitrile solution using absorption, emission, and ^{1}H NMR spectral studies, which revealed that both of the metalloreceptors act as sensors for F^-, for AcO^-, and, to some extent, for $H_2PO_4^-$. At a relatively lower concentration of anions, a 1:1 hydrogen-bonded adduct was formed; however, in the presence of an excess of anions, stepwise deprotonation of the two benzimidazole NH fragments occurred, an event that was signaled by the development of vivid colors visible with the naked eye. Double deprotonation was also observed in the presence of hydroxide. Less basic anions (AcO^- and $H_2PO_4^-$) induce deprotonation of only one NH. The effect of solvents on the absorption and emission spectral behavior has also been studied in detail. The binding affinities of different anions toward the receptors were evaluated and showed that the binding constants of **1** and **2** are substantially enhanced relative to free H_3Imbzim because upon coordination to the Ru^{II} center(s), H_3Imbzim/H_2Imbzim$^-$ becomes electron-deficient, thereby rendering the imidazole NH protons more available for hydrogen bonding to the anions. Cyclic voltammetry studies carried out in acetonitrile provided evidence of an anion-dependent electrochemical response with F^- and AcO^-. Anion-induced lifetime shortening makes complex **2** a suitable lifetime-based sensor for anions.

Introduction

The recognition and sensing of anions has emerged recently as a key research area within the generalized area of supramolecular chemistry for the important role played by anions in biological, industrial, and environmental processes.[1−8] For example, the majority of enzymes bind anions as either substrates or cofactors, and many anions act as ubiquitous nucleophiles, bases, redox agents, and phase-transfer catalysts.[9,10] It is believed that many diseases such as cystic fibrosis and Alzheimer's diseases are induced by the malfunction of natural anion regulation processes.[11,12] Environmentally, the eutrophication of water is caused by phosphate and nitrate ions used in agricultural fertilizers.[13−16] Given this importance,

*To whom correspondence should be addressed: E-mail: sbaitalik@hotmail.com.

(1) (a) Sessler, J. L.; Gale, P. A.; Cho, W. S. *Anion Receptor Chemistry*; Royal Society of Chemistry: Cambridge, U.K., 2006. (b) Caltagirone, C.; Gale, P. A. *Chem. Soc. Rev.* **2009**, *38*, 520. (c) Gale, P. A.; Garcia-Garrido, S. E.; Garric, J. *Chem. Soc. Rev.* **2008**, *37*, 151. (d) Beer, P. D. *Chem. Commun.* **1996**, 689. (e) Beer, P. D.; Gale, P. A. *Angew. Chem., Int. Ed.* **2001**, *40*, 486. (f) Gale, P. A. *Coord. Chem. Rev.* **2006**, *250*, 2917. (g) Gale, P. A. *Coord. Chem. Rev.* **2003**, *240*, 226. (h) Sessler, J. L.; Davis, J. M. *Acc. Chem. Res.* **2001**, *34*, 989.

(2) (a) Martínez-Máñez, R.; Sancenón, F. *Chem. Rev.* **2003**, *103*, 4419. (b) Beer, P. D. *Coord. Chem. Rev.* **2000**, *205*, 131. (c) Sun, S.-S.; Lees, A. J. *Coord. Chem. Rev.* **2002**, *230*, 171. (d) Sun, S.-S.; Anspach, J. A.; Lees, A. J.; Zavalij, P. Y. *Organometallics* **2002**, *21*, 685. (e) Lin, T.-P.; Chen, C.-Y.; Wen, Y.-S.; Sun, S.-S. *Inorg. Chem.* **2007**, *46*, 9201. (f) Sun, S.-S.; Lees, A. J.; Zavalij, P. Y. *Inorg. Chem.* **2003**, *42*, 3445. (g) Sun, S.-S.; Lees, A. J. *J. Am. Chem. Soc.* **2000**, *122*, 8956. (h) Wu, C.-Y.; Chen, M.-S.; Lin, C.-A.; Lin, S.-C.; Sun, S.-S. *Chem.—Eur. J.* **2006**, *12*, 2263–2269. (i) Slone, R. V.; Yoon, D. I.; Calhoun, R. M.; Hupp, J. T. *J. Am. Chem. Soc.* **1995**, *117*, 11813. (j) Chow, C.-F.; Chiu, B. K. W.; Lam, M. H. W.; Wong, W.-Y. *J. Am. Chem. Soc.* **2003**, *125*, 7802. (k) Lee, D. H.; Im, J. H.; Son, S. U.; Chung, Y. K.; Hong, J.-I. *J. Am. Chem. Soc.* **2003**, *125*, 7752. (l) Han, M. S.; Kim, D. H. *Angew. Chem., Int. Ed.* **2002**, *41*, 3809. (m) Fabbrizzi, L.; Leone, A.; Taglietti, A. *Angew. Chem., Int. Ed.* **2001**, *40*, 3066. (n) Pelleteret, D.; Fletcher, N. C.; Doherty, A. P. *Inorg. Chem.* **2007**, *47*, 4386.

(3) (a) *Supramolecular Chemistry of Anions*; Bianchi, A., Bowman-James, K., Garcia-España, E., Eds.; Wiley-VCH: New York, 1997. (b) Bowman-James, K. *Acc. Chem. Res.* **2005**, *38*, 671.

(4) Lehn, J.-M. *Supramolecular Chemistry, Concepts and Perspective*; VCH: Weinheim, Germany, 1995.

(5) Amendola, V.; Gómez, E. D.; Fabbrizzi, L.; Licchelli, M. *Acc. Chem. Res.* **2006**, *39*, 343.

Published on Web 02/02/2010

it is not surprising that extensive studies have been dedicated to the design of simple artificial anion receptors and sensors.

Sensor molecules should fundamentally have a receptor component specific for a selected analyte and also a signaling unit to translate the analyte-binding-induced changes into an output signal. These changes could be probed through changes in ^{1}H NMR chemical shifts, redox potentials, and/or additional spectral properties.[1−8,17−20] Among the sensor molecules where changes in the spectral properties are used for probing the analyte−receptor binding, fluorescence-based sensors have received considerable attention in order to achieve the high sensitivity and low analyte detection limit. Generally, the chromophores may be organic compounds or metal−organic frameworks, and binding sites with hydrogen-bonding donors or receptors containing urea and thiourea, amide, pyrrole, and imidazole subunits have been well exploited.[1−6] Though each of these motifs presents certain advantages, there is incentive to explore additional putative binding subunits that could be used to generate new receptor systems. In our search for appropriate ligands for the construction of suitable anion sensors, we have found the 4,5-bis(benzimidazol-2-yl)imidazole[21] (H_3Imbzim) system, which has yet to be exploited in the area of anion sensor development.

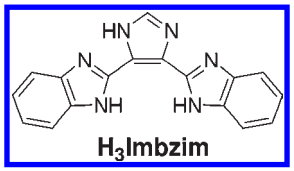

H_3Imbzim

H_3Imbzim contains three imidazole NH protons that could be donated for hydrogen bonding to the anions. It must be mentioned that the acidity of the H atom that participates in the hydrogen-bond formation with the anionic analyte is crucial. In some cases, it may not be easy to establish a clear difference between a hydrogen-bond donor binding to an anion and a process in which the hydrogen-bond donor is deprotonated and H^+ transferred to the basic anion.[5] According to a recent view, "all hydrogen bonds can be considered as incipient proton-transfer reactions, and for strong hydrogen bonds, this reaction can be in a very advanced state".[22] Thus, the nature of this process is controlled by several factors including the acidity of the receptor, the basicity of the anion, and the stability of the conjugate base, all of which are solvent-dependent.

Recently, the design and development of sensitive colorimetric sensors have received more attention owing to the facile visual recognition of a particular analyte. In this regard, metal ions can be profitably used as structural elements either for building up receptors or for assisting anion binding interaction.[2,7] The use of luminescent transition-metal complexes as sensors continues to attract considerable interest because they have relatively long lifetimes compared to their purely organic counterparts.[23−27] It is becoming clear that lifetime-based detection has significant advantages vis-à-vis intensity methods in that the lifetime methods are relatively insensitive to source variation, photobleaching of the probe material, and changes in the efficiency of the optical system. This insensitivity greatly reduces the need for repetitive calibration, a real problem for remote sensing applications.[27] Because of their excellent photochemical and redox properties,[28,29] a number of ruthenium(II) polypyridine based receptors have been designed for the construction of

(6) (a) Suksai, C.; Tuntulani, T. *Top. Curr. Chem.* **2005**, *255*, 163. (b) Suksai, C.; Tuntulani, T. *Chem. Soc. Rev.* **2003**, *32*, 192.
(7) (a) Peŕez, J.; Riera, L. *Chem. Commun.* **2008**, 533. (b) Peŕez, J.; Riera, L. *Chem. Soc. Rev.* **2008**, *37*, 2658.
(8) (a) Lam, S.-T.; Zhu, N.; Yam, V. W. W. *Inorg. Chem.* **2009**, *48*, 9664. (b) Wong, K. M. C.; Tang, W. S.; Lu, X. X.; Zhu, N.; Yam, V. W. W. *Inorg. Chem.* **2005**, *44*, 1492. (c) Yam, V. W. W.; Ko, C. C.; Zhu, N. *J. Am. Chem. Soc.* **2004**, *126*, 12734.
(9) Kirk, K. L. *Biochemistry of the Halogens and Inorganic Halides*; Plenum Press: New York, 1991; p 58.
(10) (a) *The Biochemistry of the Nucleic Acids*, 10th ed.; Adams, R. L. P., Knowler, J. T., Leader, D. P., Eds.; Chapman and Hall: New York, 1986. (b) Schmidtchen, F. P. *Nachr. Chem. Technol. Lab.* **1988**, *36*, 8–17.
(11) (a) Kartner, N.; Hanraha, J. W.; Jensen, T. J.; Nalsmith, A. L.; Sun, S.; Ackerley, C. A.; Reyes, E. F.; Tsui, L.-C.; Rommens, J. M.; Bear, C. E.; Riordan, J. R. *Cell* **1991**, *64*, 681. (b) Rich, D. P.; Gregory, R. J.; Anderson, M. P.; Manavalan, P.; Smith, A. E.; Welsh, M. J. *Science* **1991**, *253*, 202.
(12) Renkawek, K.; Bosman, G. J. C. G. M. *Neuroreport* **1995**, *6*, 929–932.
(13) Moss, B. *Chem. Ind.* **1996**, 407–411.
(14) Glidewell, C. *Chem. Br.* **1990**, *26*, 137–140.
(15) Ayoob, S.; Gupta, A. K. *Crit. Rev. Environ. Sci. Technol.* **2006**, *36*, 433.
(16) Kleerekoper, M. *Endocrinol. Metab. Clin. North Am.* **1998**, *27*, 441.
(17) (a) Bondy, C. R.; Loeb, S. J. *Coord. Chem. Rev.* **2003**, *240*, 77. (b) Choi, K.; Hamilton, A. D. *Coord. Chem. Rev.* **2003**, *240*, 101. (c) Beer, P. D. *Acc. Chem. Res.* **1998**, *31*, 71. (d) Hartley, J. H.; James, T .D.; Ward, C. J. *J. Chem. Soc., Perkin Trans.* **2000**, *1*, 3155.
(18) (a) Ghosh, T.; Maiya, B.; Wong, M. W. *J. Phys. Chem. A* **2004**, *108*, 11249. (b) Mizukami, S.; Nagano, T.; Urano, Y.; Odani, A.; Kikuchi, K. *J. Am. Chem. Soc.* **2002**, *124*, 3902. (c) Anzenbacher, P., Jr.; Try, C. A.; Miyaji, H.; Jursíková, K.; Lynch, V. M.; Marquez, M.; Sessler, J. L. *J. Am. Chem. Soc.* **2000**, *122*, 10268.
(19) (a) Lu, H.; Xu, W.; Zhang, D.; Zhu, D. *Chem. Commun.* **2005**, 4777. (b) Li, Z.-B.; Lin, J.; Zhang, H.-C.; Sabat, M.; Hyacinth, M.; Pu, L. *J. Org. Chem.* **2004**, *69*, 6284. (c) Cho, E. J.; Moon, J. W.; Ko, S. W.; Lee, J. Y.; Kim, S. K.; Yoon, J.; Nam, K. C. *J. Am. Chem. Soc.* **2003**, *125*, 12376. (d) Xu, G. X.; Tarr, M. A. *Chem. Commun.* **2004**, 1050. (e) Curiel, D.; Cowley, A.; Beer, P. D. *Chem. Commun.* **2005**, 236.
(20) (a) Otón, F.; Tárraga, A.; Espinosa, A.; Velasco, M. D.; Molina, P. *J. Org. Chem.* **2006**, *71*, 4590. (b) Otón, F.; Tárraga, A.; Molina, P. *Org. Lett.* **2006**, *8*, 2107. (c) Otón, F.; Espinosa, A.; Tárraga, A.; Ramírez de Arellano, C.; Molina, P. *Chem.—Eur. J.* **2007**, *13*, 5742. (d) Otón, F.; Tárraga, A.; Velasco, M. D.; Espinosa, A.; Molina, P. *Chem. Commun.* **2004**, 1658.
(21) Takahashi, K.; Suzuki, T.; Suzuki, Y.; Takeda, H.; Zaima, T.; Mitsuhashi, K. *Nippon Kagaku Kaishi* **1974**, *8*, 595.
(22) Steiner, T. *Angew. Chem., Int. Ed.* **2001**, *41*, 48.
(23) de Silva, A. P.; Gunaratne, H. Q. N.; Gunnlaugsson, T.; Huxley, A. J. M.; McCoy, C. P.; Rademacher, J. T.; Rice, T. E. *Chem. Rev.* **1997**, *97*, 1515.
(24) Demas, J. N.; DeGraff, B. A. *Coord. Chem. Rev.* **2001**, *211*, 317.
(25) Yam, V. W. W. *Acc. Chem. Res.* **2002**, *35*, 555.
(26) Demas, J. N.; DeGraff, B. A. *Anal. Chem.* **1991**, *63*, 829A.
(27) Lakowicz, J. R. *Principles of Fluorescence Spectroscopy*, 2nd ed.; KluwerAcademic/Plenum Publishers: New York, 1999.
(28) (a) Balzani, V.; Juris, A.; Venturi, M. *Chem. Rev.* **1996**, *96*, 759. (b) Schubert, U. S.; Eschbaumer, C. *Angew. Chem., Int. Ed.* **2002**, *41*, 2893. (c) Baba, A.; Shaw, J. R.; Simon, J. A.; Thummel, R. P.; Schmehl, R. H. *Coord. Chem. Rev.* **1998**, *171*, 43. (d) Browne, W. R.; Hage, R.; Vos, J. G. *Coord. Chem. Rev.* **2006**, *250*, 1653. (e) Medlycott, E. A.; Hanan, G. S. *Coord. Chem. Rev.* **2006**, *250*, 1763.
(29) (a) Baitalik, S.; Wang, X.; Schmehl, R. H. *J. Am. Chem. Soc.* **2004**, *126*, 16304. (b) Wang, X.; Del Guerzo, A.; Baitalik, S.; Simon, G.; Shaw, G. B.; Chen, L. X.; Schmehl, R. H. *Photosynth. Res.* **2006**, *87*, 83. (c) Baitalik, S.; Flörke, U.; Nag, K. *Inorg. Chem.* **1999**, *38*, 3296. (d) Baitalik, S.; Flörke, U.; Nag, K. *J. Chem. Soc., Dalton Trans.* **1999**, 719. (e) Baitalik, S.; Bag, P.; Flörke, U.; Nag, K. *Inorg. Chim. Acta* **2004**, *357*, 699. (f) Baitalik, S.; Flörke, U.; Nag, K. *Inorg. Chim. Acta* **2002**, *337*, 439. (g) Baitalik, S.; Dutta, B.; Nag, K. *Polyhedron* **2004**, *23*, 913. (h) Baitalik, S.; Bag, P.; Nag, K. *Polyhedron* **2002**, *21*, 2481.

a variety of anion sensors.[30−42] However, sensors based on di- or polynuclear metal complexes are relatively sparse in the literature.[2,32,36] Moreover, the synthesis of bi- and/or polymetallic ruthenium(II) complexes with bidentate chelating units is almost invariably associated with the formation of diastereoisomers; most of the earlier physicochemical studies reported in the literature were made with mixtures.[43−45] Lately, the spatial influences of the stereoisomers on physicochemical properties have been recognized.[29c−f,43−45] Toward this end, we report herein mixed-ligand monometallic and diasteroisomerically pure bimetallic ruthenium(II) complexes derived from 2,2′-bipyridine (bpy) and H_3Imbzim for colorimetric recognition of ions such as F^- among halides and AcO^- and $H_2PO_4^-$ among oxoanions. The bridging imidazole ligand has a bifunctionality: the imines moieties can be coordinated to $Ru^{II}(bpy)_2$ fragments as a first-coordination sphere, and the imidazole NH protons in the second-coordination sphere may donate hydrogen bonds to the anions (Scheme 1). It displays vivid colors when the binding event takes place on the second sphere.

Scheme 1

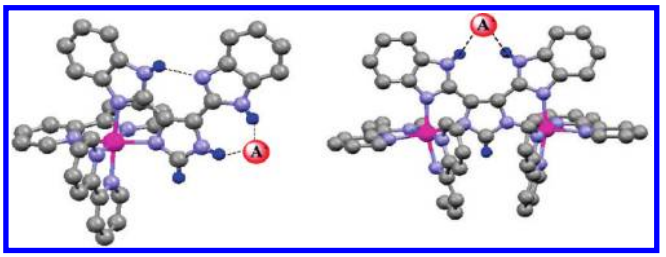

Experimental Section

Materials. Reagent-grade chemicals obtained from commercial sources were used as received. Solvents were purified and dried according to standard methods.[46] Imidazole-4,5-dicarboxylic acid was purchased from Sigma-Aldrich. *cis*-$[Ru(bpy)_2Cl_2]\cdot 2H_2O$[47] was prepared by the literature method. $AgClO_4$ was prepared from silver carbonate and perchloric acid and recrystallized from benzene.

Preparation of the Ligand H_3Imbzim. A mixture of *o*-phenylenediamine (2.7 g, 25 mmol) and 4,5-imidazoledicarboxylic acid (1.56 g, 10 mmol) in syrupy *o*-phosphoric acid (25 mL) was heated first at 220 °C for 2 h and then at 250 °C for another 2 h. The deep-blue viscous solution was cooled to room temperature and poured into crushed ice (1 L) with vigorous stirring. The blue precipitate thus obtained was filtered off. It was then slurried with water (ca. 200 mL) and slowly treated with 25% aqueous ammonia to pH ≈ 8, when the color changed to light pink. The solid was collected by filtration and washed several times with water. This was dissolved in a minimum quantity of hot *N*,*N*-dimethylformamide (DMF), stirred with a small amount of activated charcoal, and then filtered. To the filtrate was added water in small portions with stirring, and the product deposited as an off-white solid. This was recrystallized once again from a DMF/H_2O mixture. Yield: 1.35 g (45%). Mp: > 300 °C. Anal. Calcd for $C_{17}H_{12}N_6$: C, 67.99; H, 4.03; N, 27.98. Found: C, 67.69; H, 3.94; N, 27.78. ^{1}H NMR {300 MHz, DMSO-d_6, TMS, δ (ppm)} (Figure S1 in the Supporting Information): 15.85 [s, 1H, NH (central imidazole)], 8.08 (s, 1H, H7), 7.94 (d, 2H, J = 6.6 Hz, H14), 7.63 (d, 2H, J = 6.0 Hz, H11), 7.28 (m, 4H, H12 + H13). UV−vis [CH_3CN/DMF (9:1); λ_{max}, nm (ε, M^{-1} cm^{-1})]: 361 (28 250), 341 (32 200), 326 (20 100), 292 (14 900), 284 (16 800), 238 (168 000).

Preparation of the Metal Complexes. The complexes were prepared under oxygen and moisture-free dinitrogen using standard Schlenk techniques.

Caution! *$AgClO_4$ and perchlorate salts of the metal complexes used in this study are potentially explosive and therefore should be handled in small quantities with care.*

$[(bpy)_2Ru(H_3Imbzim)](ClO_4)_2\cdot 2H_2O$ (1). To a stirred suspension of *cis*-$[Ru(bpy)_2Cl_2]\cdot 2H_2O$ (0.52 g, 1 mmol) in ethanol (50 mL) was added solid $AgClO_4$ (0.42 g, 2 mmol). After 0.5 h, the precipitated AgCl was removed by filtration and the filtrate was treated with solid H_3Imbzim (0.36 g, 1.2 mmol) and 0.5 mL of 10^{-4} M $HClO_4$. The mixture was heated under reflux for 10 h with continuous stirring, after which it was filtered to remove the unreacted ligand. The filtrate upon rotary evaporation gave an orange-red crystalline product, which was collected by filtration. The compound was recrystallized from methanol/water (5:1) containing a few drops of 10^{-4} M $HClO_4$. Yield: 0.62 g (65%). Anal. Calcd for $C_{37}H_{32}N_{10}Cl_2O_{10}Ru$: C, 46.84; H, 3.40; N, 14.76. Found: C, 46.71; H, 3.47; N, 14.65. ^{1}H NMR {300 MHz, DMSO-d_6, TMS, δ (ppm)}: 14.44 [1H, NH (central imidazole)], 13.56 [1H, NH (metal-coordinated benzimidazole

(30) Anzebacher, P.; Tyson, D. S.; Jurslkova, K.; Castellano, F. N. *J. Am. Chem. Soc.* **2002**, *124*, 6232.
(31) Mizuno, T.; Wei, W.-H.; Eller, L. R.; Sessler, J. L. *J. Am. Chem. Soc.* **2002**, *124*, 1134.
(32) (a) Beer, P. D.; Szemes, F.; Balzani, V.; Salà, C. M.; Drew, M. G. B.; Dent, S. W.; Maestri, M. *J. Am. Chem. Soc.* **1997**, *119*, 11864. (b) Beer, P. D.; Graydon, A. R.; Sutton, L. R. *Polyhedron* **1996**, *15*, 2457. (c) Beer, P. D.; Szemes, F. *J. Chem. Soc., Chem. Commun.* **1995**, 2245. (d) Beer, P. D.; Dent, S. W.; Fletcher, N. C.; Wear, T. J. *Polyhedron* **1996**, *15*, 2983. (e) Beer, P. D.; Timoshenko, V.; Maestri, M.; Passaniti, P.; Balzani, V. *Chem. Commun.* **1999**, 1755. (f) Beer, P. D.; Drew, M. G. B.; Hesek, D.; Jagessar, R. *J. Chem. Soc., Chem. Commun.* **1995**, 1187. (g) Beer, P. D.; Mortimer, R. J.; Stradiotto, N. R.; Szemes, F.; Weightman, J. S. *Anal. Commun.* **1995**, *32*, 419. (h) Szemes, F.; Hesek, D.; Chen, Z.; Dent, S. W.; Drew, M. G. B.; Goulden, A. J.; Graydon, A. R.; Grieve, A.; Mortimer, R. J.; Wear, T. J.; Weightman, J. S.; Beer, P. D. *Inorg. Chem.* **1996**, *35*, 5868.
(33) (a) Cui, Y.; Mo, H.-J.; Chen, J.-C.; Niu, Y.-L.; Zhong, Y.-R.; Zheng, K.-C.; Ye, B.-H. *Inorg. Chem.* **2007**, *46*, 6427. (b) Cui, Y.; Niu, Y.-L.; Cao, M. L.; Wang, K.; Mo, H.-J.; Zhong, Y.-R.; Ye, B.-H. *Inorg. Chem.* **2008**, *47*, 5616. (c) Ye, B.-H.; Ding, B.-B.; Weng, Y.-Q.; Chen, X.-M. *Inorg. Chem.* **2004**, *43*, 6866. (d) Ding, B.-B.; Weng, Y.-Q.; Mao, Z.-W.; Lam, C.-K.; Chen, X.-M.; Ye, B.-H. *Inorg. Chem.* **2005**, *44*, 8836. (e) Ding, B.-B.; Weng, Y.-Q.; Cui, Y.; Chen, X.-M.; Ye, B.-H. *Supramol. Chem.* **2005**, *17*, 475.
(34) (a) Lin, Z.-H.; Ou, S.-J.; Duan, C.-Y.; Zhang, B.-G.; Bai, Z.-P. *Chem. Commun.* **2006**, 624. (b) Lin, Z.-H.; Zhao, Y.-G.; Duan, C.-Y.; Zhang, B.-G.; Bai, Z.-P. *Dalton Trans.* **2006**, 3678.
(35) Ion, L.; Morales, D.; Perez, J.; Riera, L.; Riera, V.; Kowenicki, R. A.; McPartlin, M. *Chem. Commun.* **2006**, 91.
(36) Zapata, F.; Caballero, A.; Espinosa, A.; Tárraga, A.; Molina, P. *J. Org. Chem.* **2008**, *73*, 4034.
(37) (a) Derossi, S.; Adams, H.; Ward, M. D. *Dalton Trans.* **2007**, 33. (b) Lazarides, T.; Miller, T. A.; Jeffery, J. C.; Ronson, T. K.; Adams, H.; Ward, M. D. *Dalton Trans.* **2005**, 528.
(38) Jose, D. A.; Kar, P.; Koley, D.; Ganguly, B.; Thiel, W.; Ghosh, H. N.; Das, A. *Inorg. Chem.* **2007**, *46*, 5576.
(39) Rau, S.; Buttner, T.; Temme, C.; Ruben, M.; Gorls, H.; Walther, D.; Duati, M.; Fanni, S.; Vos, J. G. *Inorg. Chem.* **2000**, *39*, 1621.
(40) Fortin, S.; Beauchamp, A. L. *Inorg. Chem.* **2001**, *40*, 105.
(41) Watanabe, S.; Onogawa, O.; Komatsu, Y.; Yoshida, K. *J. Am. Chem. Soc.* **1998**, *120*, 229.
(42) Aoki, S.; Zulkefeli, M.; Shiro, M.; Kohsako, M.; Takeda, K.; Kimura, E. *J. Am. Chem. Soc.* **2005**, *127*, 9129.
(43) (a) D'Alessandro, D. M.; Keene, R. F. *Chem. Soc. Rev.* **1998**, *27*, 185. (b) D'Alessandro, D. M.; Keene, F. R. *Chem.—Eur. J.* **2005**, *11*, 3679.
(44) (a) Bodige, S.; Kim, M.-J.; MacDonnell, F. M. *Coord. Chem. Rev.* **1999**, *185/186*, 535. (b) Kim, M.-J.; MacDonnell, F. M.; Gimon- Kinsel, M. E.; DuBois, T.; Asgharian, N.; Griener, J. C. *Angew. Chem., Int. Ed.* **2000**, *39*, 615.
(45) (a) Hua, X.; von Zelewsky, A. *Inorg. Chem.* **1991**, *30*, 3796. (b) Hayoz, P.; von Zelewsky, A.; Stoeckli-Evans, H. *J. Am. Chem. Soc.* **1993**, *115*, 5111. (c) Hua, X.; von Zelewsky, A. *Inorg. Chem.* **1995**, *34*, 5791. (d) Knof, U.; von Zelewsky, A. *Angew. Chem., Int. Ed.* **1999**, *38*, 302.
(46) Perrin, D. D.; Armarego, W. L.; Perrin, D. R. *Purification of Laboratory Chemicals*, 2nd ed.; Pergamon: Oxford, U.K., 1980.
(47) Sullivan, B. P.; Meyer, T. J. *Inorg. Chem.* **1978**, *17*, 3334.

site)], 12.74 [1H, NH (free benzimidazole site)], 8.84−8.80 (m, 3H, H3), 8.75 (d, 1H, J = 8.0 Hz, H3), 8.22 (t, 1H, J = 7.3 Hz, H4), 8.17 (d, 1H, J = 5.0 Hz, H6), 8.15−8.10 (m, 3H, H4), 8.08−8.04 (m, 4H, H11 + 2H5 + H7), 7.98 (d, 1H, J = 5.5 Hz, H6), 7.84 (d, 1H, J = 5.5 Hz, H6), 7.58 (t, 1H, J = 6.8 Hz, H5), 7.53 (t, 1H, J = 6.5 Hz, H5), 7.51−7.48 (m, 3H, nr, H6 + H12′ + H13′), 7.40−7.38 (m, 2H, nr, H11′ + H14′), 7.34 (t, 1H, J = 7.8 Hz, H12), 7.02 (t, 1H, J = 7.8 Hz, H13), 5.62 (d, 1H, J = 8.5 Hz, H14). ESI-MS (positive, CH_3CN): m/z 356.97 (45%) $[(bpy)_2Ru(H_3Imbzim)]^{2+}$, 712.92 (100%) $[(bpy)_2Ru(H_2Imbzim)]^{+}$. UV−vis [$CH_3CN$; λ_{max}, nm (ε, M^{-1} cm^{-1})]: 475 (9230), 425 (10 070), 357 (31 500), 339 (30 310), 290 (68 750), 242 (40 500).

$[(bpy)_2Ru(H_2Imbzim)Ru(bpy)_2](ClO_4)_3 \cdot 2H_2O$ (2). A solution of $[Ru(bpy)_2(Et\ OH)_2]^{2+}$ was prepared by stirring a mixture of *cis*-$[Ru(bpy)_2Cl_2]\cdot 2H_2O$ (0.52 g, 1 mmol) and $AgClO_4$ (0.42 g, 2 mmol) in ethanol (50 mL) for 0.5 h and removing the AgCl that precipitated. To the filtrate were added $H_3Imbzim$ (0.15 g, 0.5 mmol) and triethylamine (0.05 g, 0.5 mmol), and the solution was refluxed for 8 h, during which time the color changed from blood-red to orange-red. Upon cooling, the orange crystalline compound that deposited was collected by filtration and recrystallized from a methanol/acetonitrile (2:1) mixture. Yield: 0.45 g (63%). Anal. Calcd for $C_{57}H_{47}N_{14}Cl_3O_{14}Ru_2$: C, 46.86; H, 3.22; N, 13.43. Found: C, 46.69; H, 3.16; N, 13.65. ^{1}H NMR {300 MHz, DMSO-d_6, TMS, δ (ppm)}: 13.61 [s, 2H, NH (benzimidazole)], 8.85 (d, 2H, J = 8.1 Hz, H3), 8.77 (d, 2H, J = 8.1 Hz, H3), 8.72 (d, 2H, J = 8.1 Hz, H3), 8.64 (d, 2H, J = 8.0 Hz, H3), 8.41 (d, 2H, J = 5.1 Hz, H6), 8.19 (t, 2H, J = 7.5 Hz, H4), 8.11−8.05 (m, 6H, nr, 4H4 + 2H6), 7.99 (t, 2H, J = 7.4 Hz, H4), 7.76 (d, 2H, J = 8.0 Hz, H11), 7.64 (d, 2H, J = 5.3 Hz, H6), 7.57 (t, 2H, J = 6.6 Hz, H5), 7.55−7.50 (m, 4H, 2H5 + 2H6), 7.30 (m, 4H, H5), 7.19 (t, 2H, J = 6.7 Hz, H12), 6.97 (t, 2H, J = 7.5 Hz, H13), 5.56 (d, 2H, J = 8.1 Hz, H14), 5.12 (s, 1H, H7). UV−vis [CH_3CN; λ_{max}, nm (ε, M^{-1} cm^{-1})]: 488 (12 500), 447 (13 300), 367 (34 100), 290 (104 800), 242 (74 100).

Alternative Route for 2. A mixture of *cis*-$[Ru(bpy)_2Cl_2]\cdot 2H_2O$ (0.57 g, 1 mmol), $H_3Imbzim$ (0.15 g, 0.5 mmol), and triethylamine (0.05 g, 0.5 mmol) in 100 mL of ethanol/water (1:1) was heated under reflux with continuous stirring for 24 h under dinitrogen protection. The solution was filtered, and to the cooled filtrate (ca. 5 °C) was added an aqueous solution (5 mL) of NH_4PF_6 (1 g). After the mixture was stirred for 10 min, the red-orange shiny, microcrystalline compound that deposited was filtered. The product was recrystallized twice from a methanol/acetonitrile (2:1) mixture. Anal. Calcd for $C_{57}H_{47}N_{14}P_3F_{18}O_2Ru_2$: C, 42.86; H, 2.97; N, 12.28. Found: C, 42.73; H, 3.07; N, 12.11. ESI-MS (positive, CH_3CN): m/z 375.02 (6%) $[(bpy)_2Ru(H_2Imbzim)Ru(bpy)_2]^{3+}$, 563.0 (100%) $[(bpy)_2Ru(HImbzim)Ru(bpy)_2]^{2+}$, 1270.52 (10%) $[(bpy)_2Ru(HImbzim)Ru(bpy)_2(PF_6)]^{+}$.

Physical Measurements. Elemental (C, H, and N) analyses were performed on a Perkin-Elmer 2400II analyzer. Electrospray ionization mass spectrometry (ESI-MS) spectra were obtained on a Micromass Qtof YA 263 mass spectrometer.

^{1}H and {^{1}H−^{1}H} COSY spectra were obtained at room temperature on a Bruker Avance DPX 300 spectrometer using DMSO-d_6 solutions. For the AcO^- ion titration, 3 μL aliquots of $[Bu_4N]AcO$ (0.2 M in DMSO-d_6) were added to a DMSO-d_6 solution of **1** (2.5×10^{-3} M). For the F^- ion titration, 2 μL aliquots of $[Bu_4N]F$ (0.2 M in DMSO-d_6) were added to a DMSO-d_6 solution of **2** (2.0×10^{-3} M).

Electronic absorption spectra were obtained with a Shimadzu UV 1800 spectrophotometer at room temperature. Quartz cuvettes with 1 cm path length and 3 mL volume were used for all measurements. For a typical titration experiment, 4 μL aliquots of tetrabutylammonium (TBA) salts of F^-, Cl^-, Br^-, I^-, NO_3^-, ClO_4^-, AcO^-, $H_2PO_4^-$, and HO^- (4.0×10^{-3} M in CH_3CN) were added to a 2.5 mL solution of **1** and **2** (1.5×10^{-5} M in CH_3CN) by a micropipet. Because of the limited solubility of the ligand in pure CH_3CN, the above titration experiments for $H_3Imbzim$ were carried out in the presence of a small amount of DMF. After calculation of the concentrations of the respective species, the binding constants were evaluated from the collected absorbance data of the titration curve at the specified wavelength and eq 1,[48]

$$A_{obs} = (A_0 + A_\infty K[G]_T)/(1 + K[G]_T) \quad (1)$$

where A_{obs} is the observed absorbance, A_0 is the absorbance of the free receptor, A_∞ is the maximum absorbance induced by the presence of a given anionic guest, $[G]_T$ is the total concentration of the guest, and K is the binding constant of the host−guest entity. Binding constants were performed in duplicate, and the average is reported. All data were manipulated by using the *Microcal Origin 6.0* software package.

Emission spectra were recorded on a Perkin-Elmer LS 55 fluorescence spectrometer. The room temperature (298 K) spectra were obtained in air-equilibrated CH_3CN solutions using a 1-cm-path-length quartz cell. Emission titration experiments were carried out with the same solutions as those used with absorption titration. For all luminescence measurements of metalloreceptors, excitation and emission slit widths of 10 and 15 nm were used. Quantum yields of the complexes were determined in freeze−pump−thaw-degassed solutions of the complexes by a relative method using $[Ru(bpy)_3]^{2+}$ in the same solvent as the standard.[49] The quantum yields were calculated using eq 2,[50]

$$\Phi_r = \Phi_{std}\frac{A_{std}}{A_r}\frac{I_r}{I_{std}}\frac{{\eta_r}^2}{{\eta_{std}}^2} \quad (2)$$

where Φ_r and Φ_{std} are the quantum yields of unknown and standard samples (Φ_{std} = 0.089[51] (at 298 K) in CH_3CN at λ_{ex} = 450 nm), A_r and A_{std} (< 0.1) are the solution absorbances at the excitation wavelength (λ_{ex}), I_r and I_{std} are the integrated emission intensities, and η_r and η_{std} are the refractive indices of the solvent. Experimental errors in the reported luminescence quantum yields were about 20%.

Time-correlated single-photon-counting (TCSPC) measurement was done for recording of the luminescence decay profile for the bridging ligand, $H_3Imbzim$, and their ruthenium(II) complexes **1** and **2** in CH_3CN. Air-equilibrated solutions were used for recording of the luminescence lifetime. For the TCSPC measurements, the samples were excited at 440 nm for the metal complexes and at 345 nm for the ligand $H_3Imbzim$, using a picosecond diode laser (IBH Nanoled-07) in an IBH Fluorocube apparatus. The typical full width at half-maximum (fwhm) of the system response using a liquid scatter is about 90 ps. The repetition rate is 1 MHz. For the receptor **2**, the lifetime was recorded as a function of tetrabutylammonium fluoride (TBAF) and the emission at 685 nm was monitored as a function of time. The fluorescence decays were collected on a Hamamatsu MCP photomultiplier (R3809). The fluorescence decays were analyzed using IBH DAS6 software. The following expression was used to analyze the experimental time-resolved fluorescence decays, $P(t)$:

$$P(t) = b + \sum_i^n \alpha_i \exp(-t/\tau_i) \quad (3)$$

(48) Schneider, H.-J.; Yatsimirsky, A. *Principles and Methods in Supramolecular Chemistry*; John Wiley and Sons: London, 2000; p 142.
(49) Sullivan, B. P.; Salmon, D. J.; Meyer, T. J.; Peedrin, J. *Inorg. Chem.* **1979**, *18*, 3369.
(50) van Houten, J.; Watts, R. J. *J. Am. Chem. Soc.* **1976**, *98*, 4853.
(51) (a) Cook, M. J.; Lewis, A. P.; McAuliffe, G. S. G.; Sharda, V.; Thomson, A. J.; Glasper, J. L.; Robbins, D. J. *J. Chem. Soc., Perkin Trans. 2* **1984**, 1293. (b) Crosby, G. A.; Elfring, W. H., Jr. *J. Phys. Chem.* **1976**, *80*, 2206.

Table 1. Crystallographic Data for **1** and **2**

	1	**2**
formula	$C_{37}H_{28}C_{12}N_{10}O_9Ru$	$C_{59}H_{47}Cl_7N_{14}O_{12}Ru_2$
fw	928.66	1594.40
T (K)	100(2)	100(2)
cryst syst	triclinic	monoclinic
space group	$P\bar{1}$	$P2(1)/m$
a (Å)	9.476(5)	12.589(4)
b (Å)	12.977(5)	20.331(6)
c (Å)	16.818(5)	12.818(4)
α (deg)	97.114(5)	90
β (deg)	93.968(5)	92.238(10)
γ (deg)	91.541(5)	90
V (Å^3)	2046.0(15)	3278.1(18)
D_c (g cm^{-3})	1.507	1.615
Z	2	2
μ (mm^{-1})	0.579	0.817
$F(000)$	940	1604
θ range (deg)	1.22−25.06	1.59−25.44
data/restraints/param	7206/0/586	6210/0/439
GOF on F^2	0.979	1.016
R1[a] [$I > 2\sigma(I)$], wR2[b] (all data)	0.0579, 0.1521	0.0694, 0.1817
$\Delta\rho_{max}/\Delta\rho_{min}$ (e Å^{-1})	0.946/−0.835	1.749/−0.934

[a] $R1(F) = [\sum||F_o| - |F_c||/\sum|F_o|]$. [b] $wR2(F^2) = [\sum w(F_o^2 - F_c^2)^2/\sum w(F_o^2)^2]^{1/2}$.

Here n is the number of discrete emissive species, b is a baseline correction (direct-current offset), and α_i and τ_i are the preexponential factors and excited-state fluorescence lifetimes associated with the ith component, respectively. For biexponential decays ($n = 2$), the average lifetime, $\langle\tau\rangle$, was calculated from

$$\langle\tau\rangle = \sum_{i=1}^{2} \alpha_i\tau_i^2 / \sum_{i=1}^{2} \alpha_i\tau_i \quad (4)$$

The electrochemical measurements were carried out with a BAS 100B electrochemistry system. A three-electrode assembly (BAS) comprising a platinum (for oxidation) or glassy carbon (for reduction) working electrode, platinum auxiliary electrode, and an aqueous Ag/AgCl reference electrode was used. The cyclic voltammetry (CV) and Osteryoung square-wave voltammetry (OSWV) measurements were carried out at 25 °C in CH_3CN solutions of the complex (ca. 1 mM), and the concentration of the supporting electrolyte (TEAP/TBAP) was maintained at 0.1 M. All of the potentials reported in this study were referenced against the Ag/AgCl electrode, which under the given experimental conditions gave a value of 370 (±5) mV for the ferrocene/ferrocinium couple (ΔE_p = 60 mV). The potentials recorded were automatically compensated for by the iR drop in the cell. For a typical titration experiment, 25 μL aliquots of TBA salts of the anions (2.0×10^{-2} M in CH_3CN) were added to a 5 mL (1.0×10^{-3} M) solution of sensors **1** and **2** in CH_3CN by a micropipet.

X-ray Crystal Structure Determination. Crystals suitable for structure determination were obtained by diffusing toluene and hexane into a solution of **1** and **2** in acetonitrile/dichloromethane (1:4), respectively. X-ray diffraction data for crystals of **1** and **2** mounted on a glass fiber and coated with perfluoropolyether oil were collected on a Bruker-AXS SMART APEX II diffractometer at 100 K equipped with a CCD detector using graphite-monochromated Mo Kα radiation (λ = 0.710 73 Å). Crystallographic data and details of the structure determination are summarized in Table 1. The data were processed with *SAINT*,[52] and absorption corrections were made with *SADABS*.[52] The structure was solved by direct and Fourier methods and refined by full-matrix least squares based on F^2 using *WINGX* software, which utilizes *SHELX-97*.[53] For the structure solution and refinement, the *SHELXTL* software package[54] was used. The non-H atoms were refined anisotropically, while the H atoms were placed with fixed thermal parameters at idealized positions. In the case of **1**, both of the anionic perchlorates are severely disordered and could be refined only isotropically. In both cases, the electron density maps showed the presence of some unassignable peaks, which were removed by running the program *SQUEEZE*.[55] The final least-squares refinement [$I > 200\sigma(I)$] converged to reasonably good R values, R1 = 0.0579, wR2 = 0.1381 for **1** and R1 = 0.0694(4192) and wR2 = 0.1817(6210) for **2**. The goodness of fit for **1** was 0.979, and the maximum and minimum peaks on the final difference Fourier map corresponded to +0.946 and −0.835 e Å^{-3}, respectively. The corresponding goodness of fit for **2** was 1.016, and the maximum and minimum peaks on the final difference Fourier map corresponded to +1.749 and −0.934 e Å^{-3}, respectively.

Results and Discussion

Synthesis. A modified version of the Philips method[56] was adopted for synthesis of the ligand H_3Imbzim. According to this procedure, a mixture of *o*-phenylenediamine and imidazole-4,5-dicarboxylic acid in a 2:1 molar ratio was subjected to condensation in syrupy *o*-phosphoric acid. The reaction between 1 equiv each of *cis*-[$(bpy)_2RuCl_2$] and H_3Imbzim, leading to the substitution of the two chloride ions by the two imine nitrogen donors of the incoming ligand, is kinetically slow. In terms of the reaction time and yield, the solvated cation [$(bpy)_2Ru(EtOH)_2$]$^{2+}$, generated by reacting stoichiometric amounts of *cis*-[$(bpy)_2RuCl_2$] and $AgClO_4$, acts as a better precursor relative to *cis*-[$(bpy)_2RuCl_2$] itself. Complex **1** is asymmetric because only one part of the bridging ligand H_3Imbzim is involved in metal binding, while the other part remains free. As will be seen, subsequent to complexation, the NH groups in closer proximity to the metal center become considerably more acidic relative to those in the free ligand. In particular, the probability of deprotonation of the central imidazole NH proton, and also the formation of the bimetallic complex **2**, would be enhanced. Therefore, to produce mononuclear complexes of the type [$(bpy)_2Ru^{II}(H_3Imbzim)](ClO_4)_2\cdot 2H_2O$ free from corresponding NH deprotonated species [$(bpy)_2Ru(H_2Imbzim)](ClO_4)$ and the bimetallic complex **2**, it is necessary to carry out the reaction and recrystallization process in mildly acidic conditions. The symmetrical bimetallic complex **2** is readily obtained by reacting [$(bpy)_2Ru(EtOH)_2$]$^{2+}$ with the bridging ligand H_3Imbzim and triethylamine in the ratio 2:1:1. The complexes initially isolated as mixtures of diastereoisomers were separated by fractional recrystallization from a MeOH/CH_3CN (2:1) mixture. The ESI-MS spectrum of compound **1** in CH_3CN shows (Figure S2 in the Supporting Information) two abundant peaks at m/z 356.97 and 712.92. The isotopic patterns of the original peak at m/z 356.97 separated by 0.5 Da fit very well to the isotopic distribution pattern calculated with the Mass Lynx V 4.0 program for [$(bpy)_2Ru(H_3Imbzim)$]$^{2+}$ (45%). The peak at m/z 712.92 is

(52) *SAINT*, version 6.02; Bruker AXS Inc.: Madison, WI, **2002**. *SADABS*, version 2.03; Bruker AXS Inc.: Madison, WI, **2002**.

(53) Sheldrick, G. M. *SHELXL-97, Program for the Refinement of crystal Structures*; University of Göttingen: Göttingen, Germany, **1997**.

(54) *SHELXTL*, version 6.10; Bruker AXS Inc.: Madison, WI, **2002**.

(55) Spek, A. L. PLATON. *J. Appl. Crystallogr.* **2003**, *36*, 7.

(56) Addison, A. W.; Burke, P. J. *J. Heterocycl. Chem.* **1981**, *18*, 803.

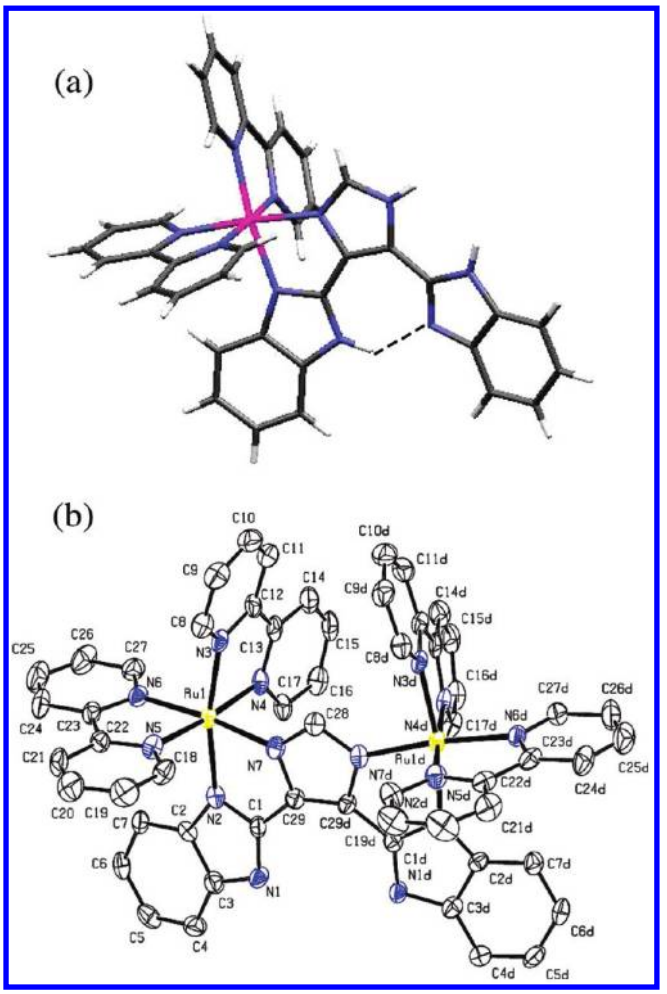

Figure 1. (a) Capped-stick projection of $\mathbf{1}^{2+}$ showing hydrogen-bonding interaction. (b) ORTEP representation of $\mathbf{2}^{3+}$ showing 50% probability of thermal ellipsoids. H atoms have been omitted for clarity.

assigned to $[(bpy)_2Ru(H_2Imbzim)]^+$ (100%). For the corresponding bimetallic complex **2**, the observed peaks at *m*/*z* 375.02, 562.99, and 1270.52 in the ESI-MS spectrum also fit very well (Figure S3 in the Supporting Information) to the isotopic distribution pattern calculated for $[(bpy)_2Ru(H_2Imbzim)Ru(bpy)_2]^{3+}$ (6%), $[(bpy)_2Ru(HImbzim)Ru(bpy)_2]^{2+}$ (100%), and $[(bpy)_2Ru(HImbzim)Ru(bpy)_2(PF_6)]^+$ (10%), respectively. The complexes were further characterized by ^{1}H NMR spectroscopy, X-ray crystallography, CV, and spectrophotometry.

Description of the Crystal Structures of 1 and 2. Complex $\mathbf{1}^{2+}$ crystallized in the triclinic form with space group $P\bar{1}$ while $\mathbf{2}^{3+}$ is in the monoclinic form with space group $P2(1)/m$. A capped-stick projection of the cation $\mathbf{1}^{2+}$ and an ORTEP view of the cation $\mathbf{2}^{3+}$ are shown in Figure 1.

Selected bond distances and angles for **1** and **2** are listed in Table 2.

The structure of **1** consists of a hexacoordinated Ru^{II} center in which the $Ru^{II}(bpy)_2$ unit is coordinated to one of the two imidazole (central) nitrogens N8 and one benzimidazole nitrogen N1 of $H_3Imbzim$. In **2**, each of the two Ru centers is coordinated by one $Ru^{II}(bpy)_2$ unit of each half of the $(H_2Imbzim^-)$ ligand and the two metal centers are bridged by one imidazolate (central) nitrogen N7 and one benzimidazole nitrogen N2. The two pyridyl

Table 2. Selected Bond Distances (Å) and Angles (deg) for **1** and **2**

1		**2**	
Ru−N6	2.033(4)	Ru−N7	2.039(5)
Ru−N4	2.039(4)	Ru−N5	2.041(5)
Ru−N3	2.039(4)	Ru−N6	2.045(5)
Ru−N5	2.074(4)	Ru−N4	2.050(5)
Ru−N8	2.077(4)	Ru−N3	2.051(5)
Ru−N1	2.093(4)	Ru−N2	2.077(5)
		Ru---Ru	6.124
N6−Ru−N4	89.20(15)	N7−Ru−N5	97.70(2)
N6−Ru−N3	96.47(16)	N7−Ru−N6	173.63(2)
N4−Ru−N3	79.21(17)	N5−Ru−N6	78.82(2)
N6−Ru−N5	78.88(17)	N7−Ru−N4	86.62(2)
N4−Ru−N5	100.60(16)	N5−Ru−N4	174.75(2)
N3−Ru−N5	175.35(16)	N6−Ru−N4	97.15(2)
N6−Ru−N8	172.98(16)	N7−Ru−N3	91.35(2)
N4−Ru−N8	95.51(15)	N5−Ru−N3	97.92(2)
N3−Ru−N8	89.54(16)	N6−Ru−N3	94.41(2)
N5−Ru−N8	95.10(17)	N4−Ru−N3	78.93(2)
N6−Ru−N1	97.48(15)	N7−Ru−N2	76.83(2)
N4−Ru−N1	170.99(15)	N5−Ru−N2	88.99(2)
N3−Ru−N1	93.97(16)	N6−Ru−N2	97.67(2)
N5−Ru−N1	86.67(15)	N4−Ru−N2	94.92(2)
N8−Ru−N1	78.42(15)	N3−Ru−N2	167.06(2)

N atoms of each bpy ligand are coordinated alternatively in axial and equatorial modes. In both compounds, three types of metal−nitrogen distances are observed. The longest Ru−N distances involve the benzimidazole N atoms, with their values being 2.093(4) Å for **1** and 2.077(5) Å for **2**. The next-longest Ru−N distance, pertaining to the central imidazole N atom, is 2.077(4) Å for **1**. However, in the bimetallic complex **2**, the corresponding distance is the shortest [2.039(5) Å] among all Ru−N distances because of the enhanced electron-accepting ability of the central imidazolate ring due to the sharing of its two N atoms by two $[Ru(bpy)_2]^{2+}$ units. The bpy ligands provide the shortest Ru−N distances [except Ru−N7 = 2.039(5) Å for **2**], with average values of 2.033(4)−2.050(5) Å. Deviation of the metal center from the idealized octahedral geometry is reflected in their bond angles: the cis angles vary from 78.42(15)° to 79.21(17)° for **1** and from 76.86(2)° to 78.92(2)° for **2**, while the trans angles vary between 170.99(15)° and 175.35(16)° for **1** and between 167.06(2)° and 174.76(2)° for **2**. The crystal structure of complex **2** clearly shows that the two Ru centers in this diastereoisomer are in the heterochiral meso (ΛΔ) form and the separation between the nonbonding Ru centers is 6.124 Å. In the structure **1**, it is seen that (Figure 1a) the NH proton of the metal-coordinated benzimidazole side is involved in an intramolecular hydrogen-bonding interaction with the N atom of the free benzimidazole moiety with a N−H---N distance of 2.096 Å. In both structures, it is seen that the two NH groups adopt a cis arrangement, and this pair of externally directed NH protons of $H_2Imbzim^-$ could be used for the formation of an adduct with anions via hydrogen-bonding interaction (Scheme 1).

^{1}H NMR Spectra. The ^{1}H and $\{^1H-^1H\}$ COSY NMR spectra for complexes **1** and **2** have been recorded in $(CD_3)_2SO$ solutions at room temperature. The numbering scheme used to assign the observed resonances is given in Scheme 2.

The ^{1}H NMR spectra for both complexes (Figures 2 and 3) show the occurrence of a fairly large number of

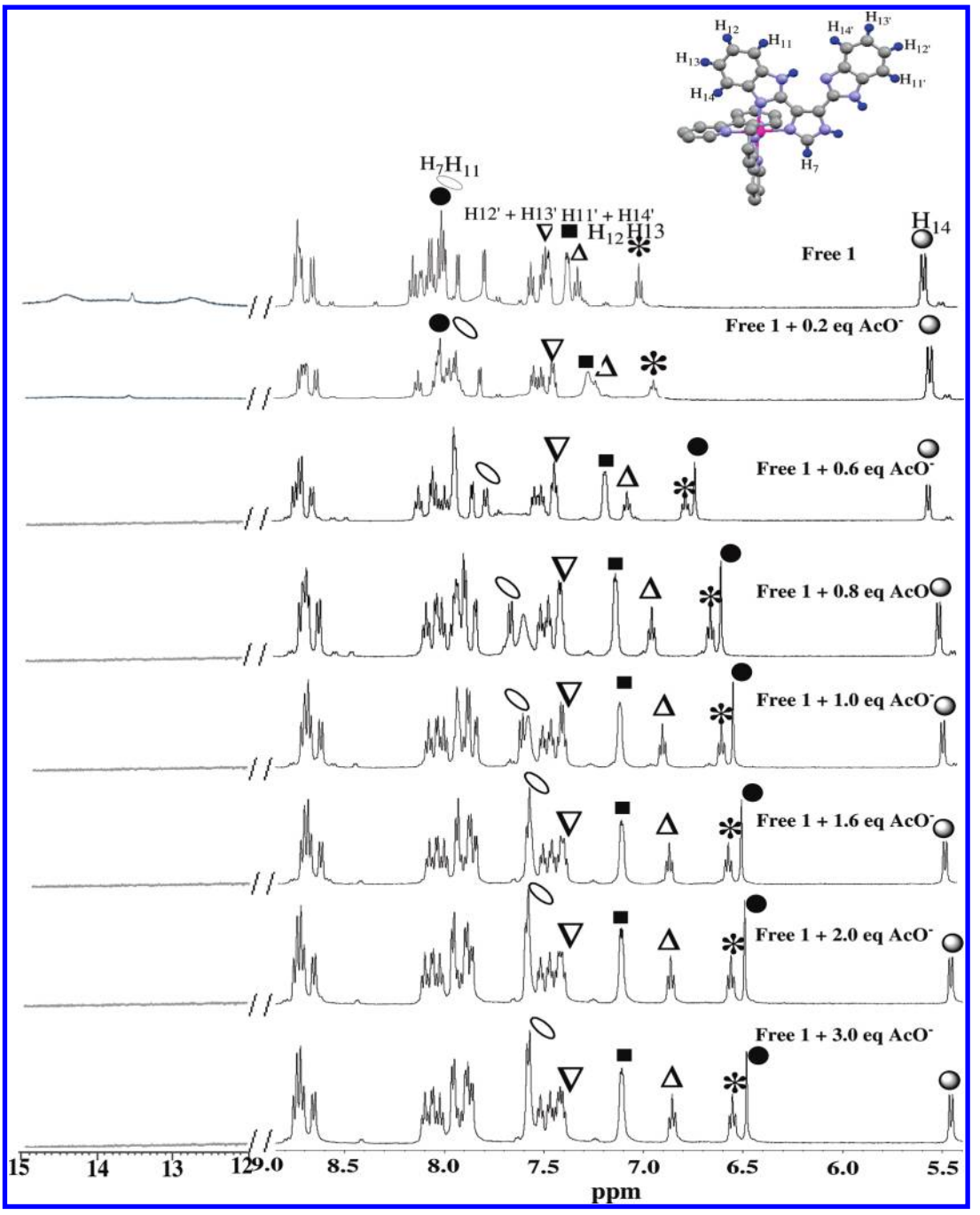

Figure 2. ^{1}H NMR titration of sensor **1** in DMSO-d_6 solution (2.5×10^{-3} M) upon addition of AcO^- ion (0−3 equivalents).

Scheme 2

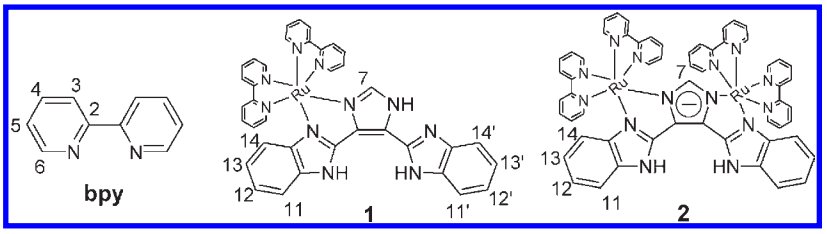

resonances, many of which are overlapped with each other. The COSY spectra have been particularly useful in locating spin couplings in the aromatic protons of the benzimidazole moiety bound to the metal versus the uncoordinated one. The assignments of the bpy protons were facilitated by taking into consideration of the following facts. Usually for $Ru(bpy)_n^{2+}$ species, the decreased order of the chemical shifts is H3 > H4 ≥ H5 > H6.

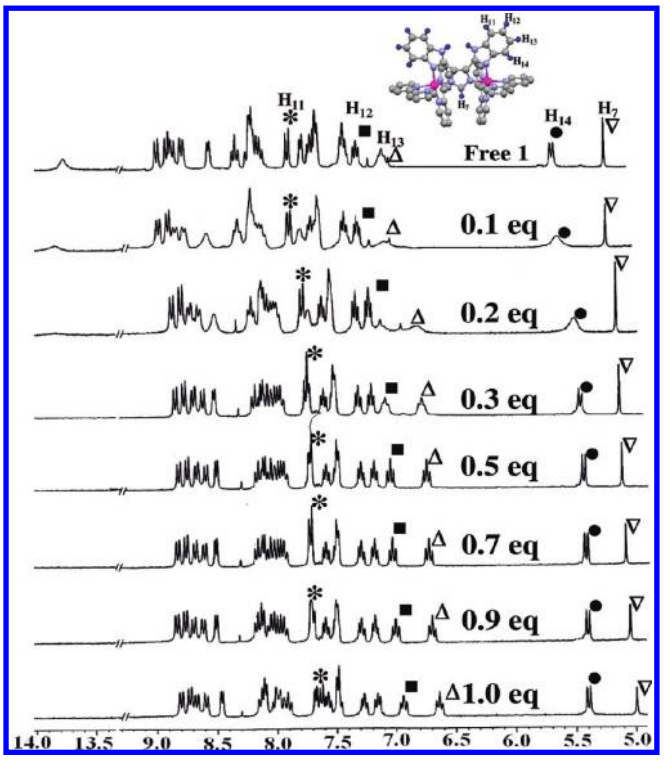

Figure 3. ^{1}H NMR titration of a 2.0×10^{-3} M solution of **2** in DMSO-d_6 upon addition of F^- ion (0−1.5 equivalents).

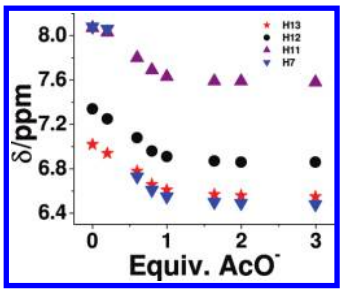

Figure 4. Change of the chemical shifts for H7, H11, H12, and H13 protons of complex **1** as a function of the equivalents of AcO^- added.

Figure 5. Color changes seen for CH_3CN solutions of the metalloreceptors **1** (a) and **2** (b) upon addition of anions as TBA salts.

The protons H3 and H6 are normally observed as doublets, while H4 and H5 appear either as a triplet or a doublet of doublet. The spin-coupling constants are $J_{3,4}$ and $J_{4,5} \approx 8$ Hz, $J_{5,6} \approx 5$ Hz, and $J_{3,5}$, and $J_{4,6} \approx 1.2$ Hz.[29] However, because of the overlapping of some of these signals, their splitting patterns get obscured. As may be seen in Figures 2 and 3, for each of the complexes, all of the resonances, barring two, occur in the range 6.55−8.85 ppm. Of the two disparate signals, the one that is most shielded among all others appears as a doublet between 5.56 and 5.62 ppm. The doublet accounts for a single proton in **1** and for two protons in **2** and is clearly due to H14 (see Scheme 2 for proton labeling) because this proton experiences maximum diamagnetic shielding by the anisotropic ring current of the adjacent bpy rings (Figure 1). The second distinct signal, which is the most downfield-shifted, is observed either as a singlet or as a broad feature in the region 12.0−15.0 ppm due to the three benzimidazole NH protons of the coordinated H_3Imbzim ligand.

To prove the interaction of metalloreceptors with various anions, ^{1}H NMR titration was carried out with increasing amounts of anions (F^-, AcO^-, and $H_2PO_4^-$ ions) to DMSO-d_6 solutions of **1** and **2**. Unfortunately, because of the limited solubility of the receptors **1** and **2** in a CD_3CN solution, experiments were carried out in a DMSO-d_6 solution. A 5.0×10^{-3} M solution of **1** in DMSO-d_6 was titrated with up to 3 equiv of a AcO^- ion. As is shown in Figure 2, three signals due to three different NH protons of the metal-coordinated H_3Imbzim ligand are observed at 12.74, 13.55, and 14.43 ppm. The imidazole NH protons are profoundly downfield-shifted because of hydrogen bonding with DMSO-d_6. Upon the gradual addition of AcO^-, the signals due to all three NH protons disappeared. The chemical shifts of the CH protons of H_3Imbzim (H7, H11, H12, H13, and H14) are also very sensitive upon addition of the anions. Upon the gradual addition of AcO^- ion to the solution of **1**, the chemical shifts of the above protons get progressively upfield-shifted. The final displacements ($\Delta\delta$) for H7, H11, H12, H13, and H14 are 1.60, 0.49, 0.48, 0.47, and 0.16 ppm, respectively. The values of the chemical shifts (δ, ppm) of different protons with varying amounts of AcO^- are summarized in Table S1 in the Supporting Information. Figure 4 shows the changes of the chemical shifts for H7, H11, H12, and H13 as a function of the equivalents of AcO^- added, with saturation being observed after the addition of ca. 1 equiv of AcO^-, indicating the formation of 1:1 complexes between **1** and AcO^-.

Furthermore, the color of the solution was seen to change from orange-yellow to violet (photograph in Figure 5a). It is interesting to note that, upon the addition of about 1 equiv of AcO^- to the solution of **1**, the singlet at δ 8.08 ppm due to H7 of the central imidazole ring of H_3Imbzim gets remarkably upfield-shifted to δ 6.48 ppm, indicating either a very strong hydrogen-bonded interaction between **1** and AcO^- or deprotonation of the NH proton of H_3Imbzim. Such a significant upfield shift of the CH proton occurs probably because of the through-bond propagation of the negative charge onto the aromatic framework generated upon NH deprotonation. The same was also found for F^- and $H_2PO_4^-$ ions.

The two NH groups of coordinated H_2Imbzim$^-$ initially appearing as a singlet at δ 13.61 ppm in the ^{1}H NMR spectrum (Figure 3) broadened, downfield-shifted to δ 13.85 ppm, and finally vanished when less than 0.5 equiv of F^- was added to a DMSO-d_6 solution of **2**, indicating a strong interaction between **2** and the F^- ion. It is

interesting to note that, like compound **1**, the signals due to H7, H11, H12, H13, and H14 protons of $H_2Imbzim^-$ upfield-shifted (Table S2 in the Supporting Information) because of the interaction of **2** and F^-. A similar behavior is also found for AcO^-. However, with $H_2PO_4^-$, the same titration was not successful because of precipitation of the complex upon the addition of the anion.

Colorimetric Signaling. The anion-sensing abilities of the receptors **1** and **2** were studied on a qualitative level by visual examination of the anion-induced color changes in CH_3CN solutions (5×10^{-5} M in CH_3CN) before and after the addition of an anion. TBA salts of F^-, Cl^-, Br^-, I^-, NO_3^-, ClO_4^-, AcO^-, and $H_2PO_4^-$ would serve as substrates for **1** and **2** in CH_3CN. The photograph in Figure 5 shows the dramatic color changes of the metallosensors **1** and **2** in the presence of F^-, AcO^-, and, to a lesser extent, $H_2PO_4^-$, suggesting strong binding. Conversely, the addition of Cl^-, Br^-, I^-, NO_3^-, and ClO_4^- induces no change in color.

Absorption Spectroscopic Studies. Complexes **1** and **2** in CH_3CN exhibit a number of absorption bands in the UV−vis region. The two most intense bands observed at around 242 and 290 nm in both complexes are due to the $\pi-\pi^*$ transition of bpy, while the next higher wavelength absorption occurring between 340 and 370 nm is due to the ligand-centered transitions of the bridging ligand. Complex **1** exhibits two fairly intense absorptions at 475 nm (ε = 9230 M^{-1} cm^{-1}) and 425 nm (ε = 10 070 M^{-1} cm^{-1}), while in **2**, these absorptions occur at 488 nm (ε = 12 500 M^{-1} cm^{-1}) and 447 nm (ε = 13 300 M^{-1} cm^{-1}), respectively. The lowest-energy absorptions are probably due to a metal-to-bridging ligand {Ru(dπ) to $H_3Imbzim/H_2Imbzim^-(\pi^*)$} charge-transfer (MLCT) transition because the $\pi-\pi^*$ transitions of the bridging ligand are lower in energy than those of bpy. The next higher energy bands are due to Ru(dπ)-to-bpy(π^*) charge-transfer (MLCT) transitions. It is seen that, upon going from a monometallic to bimetallic compound, the red shifts of the MLCT bands occur as a result of the lowering of energy of the π^* level on the bridging ligand as well as the raising of energy of the dπ orbital on Ru^{II}.

The sensing of the metalloreceptors **1** and **2** for anions was studied through UV−vis spectra in CH_3CN solutions. As can be seen from the absorption spectra, the original MLCT peaks at 475 and 425 nm for **1** (Figure 6b) and 488 and 447 nm for **2** (Figure S5 in the Supporting Information) were almost unchanged upon the addition of 8 equiv of Cl^-, Br^-, I^-, NO_3^-, and ClO_4^- anions to 1.5×10^{-5} M solutions of **1** and **2**. However, upon the addition of $H_2PO_4^-$, the MLCT bands of **1** shifted to 505 and 448 nm, but for **2**, there was almost negligible red shift except a small diminution of the intensity of the bands. Following the addition of F^- and AcO^-, the MLCT maxima were further red-shifted to 535 and 475 nm for **1** and 503 and 465 nm for **2**, respectively, demonstrating a strong interaction between the receptors and anions. Interestingly, these events can be distinguished visually, as shown in the photograph in Figure 5. The red shift

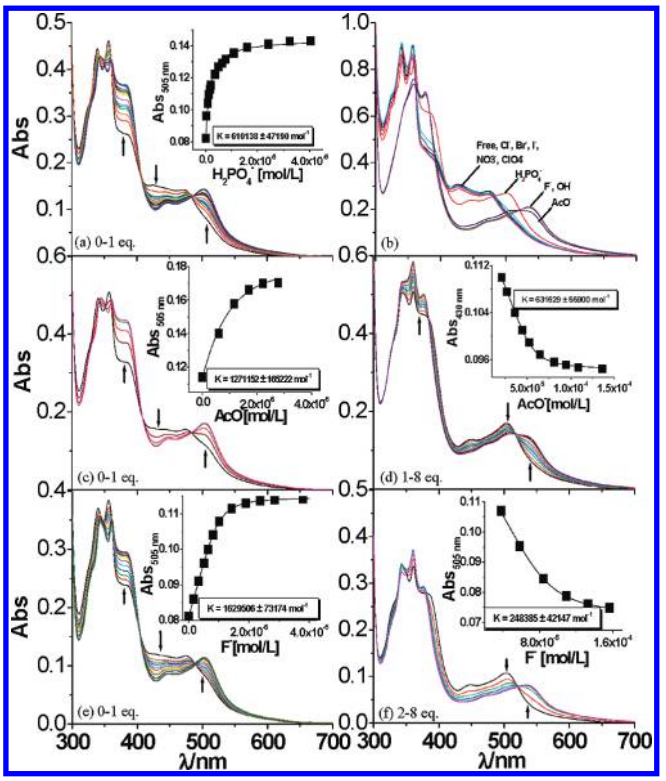

Figure 6. Changes of the UV−vis spectra of sensor **1** in CH_3CN upon the addition of (a) $H_2PO_4^-$ (0−6 equiv). (b) Different anions as TBA salts: (c) AcO^- (0−1 equiv); (d) AcO^- (1−8 equiv); (e) F^- (0−1 equiv); (f) F^- (2−8 equiv). The inset shows the fit of the experimental absorbance data to a 1:1 binding profile.

of the MLCT band can be attributed to the second-sphere donor−acceptor interactions between metal-coordinated $H_3Imbzim/H_2Imbzim^-$ and anions.[57,58] Such interactions (hydrogen-bonding or proton transfer, vide infra) increase the electron density at the metal center, resulting in a decrease of the MLCT band energy.

In order to obtain quantitative insight into sensor−anion interactions, spectrophotometric titration experiments were carried out systematically with F^-, AcO^-, and $H_2PO_4^-$. Parts c and d of Figure 6 present the changes in the UV−vis spectrum of **1** as a function of the AcO^- concentration. As can be seen from the figure, the MLCT peak at 475 nm and the shoulder at 425 nm decreased upon the addition of AcO^- to a solution of **1**, and a new peak at 505 nm and a shoulder at 448 nm appeared with two isosbestic points at 484 and 408 nm, with saturation being observed after the addition of ca. 1 equiv of AcO^- (inset to Figure 6c). Furthermore, the color of the solution was seen to change from yellow-orange to orange-brown. From Job plot analyses, these spectral changes are ascribed to the formation of 1:1 complexes between the receptor and AcO^-. Standard curve-fitting procedures were then used to derive binding constants, which are summarized in Table 3. The continuous addition of up to 8 equiv of AcO^- induces the MLCT peak at 505 nm to further decrease in intensity, and a new absorption band at 535 nm progressively developed (Figure 6d). The color of the final solution turned to violet. After that, the change of absorption spectra was negligible.

(57) Balzani, V.; Sabbatini, N.; Scandola, F. *Chem. Rev.* **1986**, *86*, 319.
(58) (a) Kang, S. O.; Powell, D.; Day, V. W.; Bowman-James, K. *Angew. Chem., Int. Ed.* **2006**, *45*, 1921. (b) Shenderovich, I. G.; Tolstoy, P. M.; Golubev, N. S.; Smirnov, S. N.; Denisov, G. S.; Limbach, H.-H. *J. Am. Chem. Soc.* **2003**, *125*, 11710.

Table 3. Equilibrium/Binding Constants[a,b] (K, M^{-1}) for **1**, **2**, and H_3Imbzim toward Various Anions in CH_3CN at 298 K

	1		**2**		H_3Imbzim
anion	K_1	K_2	K_1	K_2	K_1
			Absorption		
F^-	1.63×10^6	2.48×10^5	1.08×10^6	2.25×10^{5c}	3.31×10^4
AcO^-	1.27×10^6	6.32×10^5	1.38×10^6	1.76×10^{4c}	5.56×10^{3c}
$H_2PO_4^-$	6.10×10^5	NA[d]	$8.77 \times 10^{5\,c}$	NA	NA
OH^-	1.90×10^6	1.80×10^5	1.81×10^6	8.02×10^{4c}	6.93×10^4
			Emission		
F^-	1.00×10^6	2.58×10^5	1.45×10^6	NA	4.88×10^4
AcO^-	1.02×10^6	6.74×10^5	1.55×10^6	NA	6.80×10^{3c}
$H_2PO_4^-$	8.98×10^5	NA	8.13×10^{5c}	NA	NA
OH^-	2.23×10^6	1.91×10^5	1.79×10^6	NA	8.72×10^4

[a] *tert*-Butyl salts of the respective anions were used for the studies. [b] Estimated errors were $< 15\%$. [c] Estimate; clean binding profiles were not observed. [d] Not applicable.

A more intricate behavior is observed during the UV−vis titration of **1** upon the addition of F^-. Parts e and f of Figure 6 show the complete range of the absorption spectrum of **1** as a function of TBAF. The addition of F^- induces the peak at 475 nm and the shoulder at 425 nm to gradually decrease, and two well-defined new absorption bands at 505 and 448 nm, respectively, develop with two isosbestic points at 490 and 405 nm and reach their limiting values upon the addition of 1 equiv of F^-. With the addition of between 1 and 2 equiv of F^- to the solution of **1**, the spectral change is negligible. After that, the above MLCT peaks decrease and two new absorption bands at 535 and 475 nm with isosbestic points at 522 and 370 nm (Figure 6f) progressively develop and the color of the solution changes to violet.

Figure 6a shows the changes in the absorption spectral profile of **1** toward the $H_2PO_4^-$ ion. During the process of adding 1 equiv of $H_2PO_4^-$ to the solution of **1**, the maximum absorption peak at 475 nm gradually decreases, while a new band at 505 nm forms. A further addition of the $H_2PO_4^-$ anion gives rise to no detectable change in the absorption spectra of **1**. The appearance of two sharp isosbestic points at 481 and 407 nm in the titration profile indicates that only two species coexist at the equilibrium and form a 1:1 stoichiometry between **1** and $H_2PO_4^-$.

The above observations suggest that the first change upon the addition of 1 equiv each of AcO^-, F^-, and $H_2PO_4^-$ in the absorption spectra is a consequence of the formation of an initial hydrogen-bonding interaction between the NH protons of coordinated H_3Imbzim and the corresponding anions (A^-), followed by proton transfer to form a $\{[(bpy)_2Ru(H_2Imbzim)]\cdot HA\}^+$ association complex.[5,7,33] The equilibrium $[(bpy)_2Ru(H_3Imbzim)]^{2+} + A^- \rightleftharpoons \{[(bpy)_2Ru(H_2Imbzim)]\cdot HA\}^+$ is established, and its binding constant can be obtained via a fitting of the experimental absorbance data at 505 nm versus the concentration of the anions. Although during the addition of 1−2 equiv of AcO^- the second spectral change of **1** started, with F^-, the change in the said region was negligible. This can be considered as the formation of the highly stable HF_2^- dimer.[55] The titration profile shows that a large excess of both AcO^- and F^- is needed for the attainment of the second equilibrium process, $[(bpy)_2Ru(H_2Imbzim)]^+ + A^- \rightleftharpoons [(bpy)_2Ru(HImbzim)] + HA$, forming the bideprotonated species $[Ru(bpy)_2(HImbzim)]$. This may be attributed to an especially high pK_{a_2} value of **1** (11.0; Figure S6 in the Supporting Information). The constant K_2 is related to the second acidity constant of **1** and to the formation constant of HF_2^-. The third NH deprotonation does not occur in **1** even with a large excess of anions because of stability through intramolecular hydrogen bonding (Figure 1).

The absorption spectral changes that occur for **2** as a function of AcO^- (Figure S7 in the Supporting Information) show that, with increases of up to 1 equiv of AcO^-, the MLCT bands (488 and 447 nm) in the successive absorption curves undergo red shifts (500 and 455 nm), during which they pass through two isosbestic points at 500 and 405 nm, with saturation being observed after the addition of ca. 1 equiv of AcO^-. From Job plot analyses, these spectral changes are ascribed to the formation of 1:1 complexes between the receptor and AcO^-. Standard curve-fitting procedures were then used to derive binding constants, which are summarized in Table 3. Further additions of AcO^- up to 25 equiv induced small decreases in the intensity of these MLCT peaks until the new absorption bands at 505 and 465 nm appeared. During this second change, the absorption curves pass through a new isosbestic point at 518 nm. The change in the absorption spectral profile for **2** toward the $H_2PO_4^-$ ion is small (Figure S8 in the Supporting Information), indicating weak interaction. It may be mentioned that the addition of $H_2PO_4^-$ beyond 1 equiv gives rise to no detectable change in the absorption spectra of **2** and thereafter gives rise to precipitation of the resulting complex. The appearance of two isosbestic points at 497 and 404 nm in the titration profile indicates that only two species coexist at the equilibrium and form a 1:1 stoichiometry between **2** and $H_2PO_4^-$.

The spectral change that occurs for **2** as a function of F^- is shown in Figure 7. As the F^- ion is added to a CH_3CN solution of **2**, the MLCT absorption maxima at 488 and 447 nm get shifted to longer wavelengths, viz., 500 and 455 nm, respectively, with concurrent development of two isosbestic points at 497 and 409 nm upon the addition of 1 equiv of F^- (Figure 7a).

The continuous addition of up to 8 equiv of F^- induces these MLCT peaks to further decrease in intensity until the new absorption bands at 505 and 465 nm appeared. During this process, the absorption curves pass through two new isosbestic points at 525 and 300 nm (Figure 7c). Thus, over the entire range, the absorption maxima at 488 and 447 nm are finally shifted to 505 and 465 nm. The titration profile again suggests the presence of two distinct steps: the formation of $\mathbf{2}\cdot A^-$ interacting species through hydrogen bonding, followed by proton transfer to form a $\{[(bpy)_2Ru(HImbzim)Ru(bpy)_2]\cdot HA\}^{2+}$ association complex, which reached its limiting concentration with the addition of 1 equiv of F^-, AcO^-, and $H_2PO_4^-$ (to a lesser extent) and deprotonation of the second NH proton upon the addition of an excess (up to 8 equiv) of F^- only. The formation of bideprotonated species $\{[(bpy)_2Ru(Imbzim)Ru(bpy)_2]^+$ occurs only with a large excess of F^- and not with either AcO^- or $H_2PO_4^-$. Fitting the overall titration data by assuming the existence of two sets of equilibria gives the association constants summarized

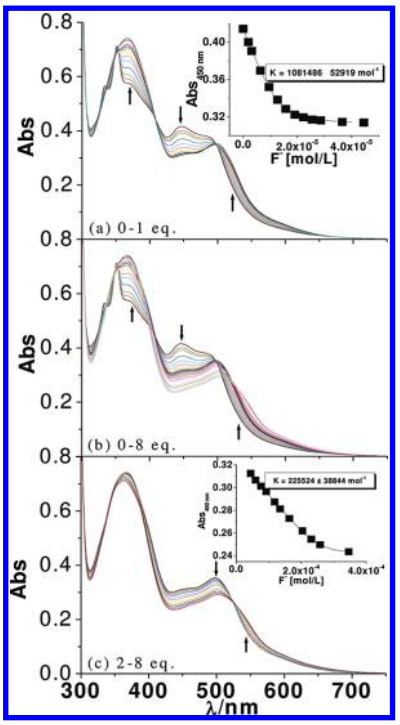

Figure 7. Changes of the UV−vis spectra of sensor **2** in CH_3CN upon the addition of F^-: (a) 0−1 equiv; (b) 0−8 equiv; (c) 2−8 equiv. The inset shows the fit of the experimental absorbance data to a 1:1 binding profile.

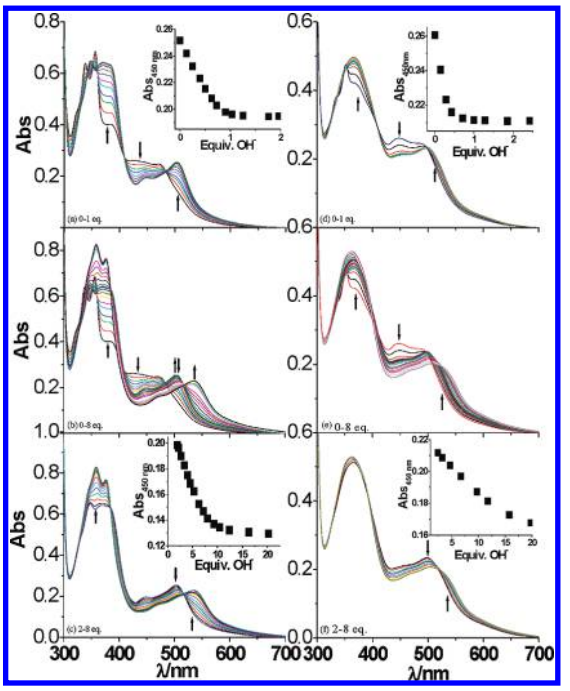

Figure 8. Changes of the UV−vis spectra in CH_3CN upon the addition of TBAOH to sensors **1** (a−c) and **2** (d−f). The inset shows the absorbance change as a function of the equivalents of OH^- added.

in Table 3. In general, **1** and **2** exhibit high sensitivity to both AcO^- and F^- but lack good selectivity to explicitly differentiate these two anions.

It was reported previously that suitably substituted hydrogen-bond-donor receptor functionality undergoes deprotonation in the presence of excess anions, leading to classical Brønsted acid−base chemistry, and is not commonly believed as a supramolecular interaction.[59−61] It has been argued that the higher stability of a polynuclear aggregate, such as HF_2^-, further facilitates deprotonation of the receptor unit. To examine such a possibility in **1** and **2**, spectrophotometric titrations of **1** and **2** (2.5×10^{-5} M) were carried out with a standard solution (5.0×10^{-3} M) of [nBu_4N]OH (Figure 8).

For **1** and **2**, the equilibrium for the hydrogen-bond formation (H−N^-···H−O) could not be distinguished; however, the proton dissociation constants could be obtained ($K_1^d = 1.9 \times 10^6$ M^{-1} and $K_2^d = 1.8 \times 10^5$ M^{-1} for **1** and $K_1^d = 1.8 \times 10^6$ M^{-1} and $K_2^d = 8.0 \times 10^4$ M^{-1} for **2**). The monodeprotonated (0−1 equiv) spectral patterns for **1** and **2** (deprotonation achieved using [nBu_4N]OH) have close resemblance to the spectra of these receptors in the presence of ca. 1 equiv each of F^- and AcO^-. Though the bideprotonated form of **1**, [$(bpy)_2$Ru(HImbzim)], can be achieved through the addition of a large excess of F^- and AcO^- as with OH^-, the corresponding bideprotonated form of **2**, [$(bpy)_2$Ru(Imbzim)Ru$(bpy)_2$]$^+$, could be obtained only with a large excess of F^- and OH^- but not with either AcO^- or $H_2PO_4^-$. These observations suggest that, in a large excess of F^- and AcO^-, the Brønsted acid−base reaction prevails, whereas in a slight excess (∼1.0 equiv), hydrogen-bonding interactions, followed by proton transfer, are operative. Observation of the third deprotonation in the case of **1** did not occur even with a huge excess of OH^- anions because of intramolecular hydrogen-bonding interaction.

It would be of interest to compare the binding ability of the free ligand H_3Imbzim with its ruthenium(II) complexes **1** and **2**. In order to do so, spectrophotometric titration experiments of H_3Imbzim in DMF/CH_3CN (1:9) with various anions were carried out. It has been observed that the interactions of the ligand occur only with F^- and, to a lesser extent, with AcO^- but not with other anions. Figure 9b presents the changes in the UV−vis spectrum of H_3Imbzim as a function of the F^- concentration.

As can be seen, the absorption peaks at 361 and 341 nm decreased upon the addition of F^- to a solution of H_3Imbzim, and a new peak at 373 nm and a shoulder at 350 nm appeared with three isosbestic points at 364, 357, and 348 nm, after the addition of a large excess of F^-. No visual change of color was observed. Standard curve-fitting procedures were then used to derive binding constants, which are summarized in Table 3. Spectrophotometric titrations of the ligand (1.5×10^{-5} M) were also carried out with a standard solution of [nBu_4N]OH. The spectral patterns obtained with OH^- (Figure 9a)

(59) (a) Boiocchi, M.; Del Boca, L.; Gomez, D. E.; Fabbrizzi, L.; Licchelli, M.; Monazani, E. *J. Am. Chem. Soc.* **2004**, *126*, 16507. (b) Gomez, D. E.; Fabbrizzi, L.; Licchelli, M.; Monazani, E. *Org. Biomol. Chem.* **2005**, *3*, 1495.

(60) (a) Peng, X.; Wu, Y.; Fan, J.; Tian, M.; Han, K. *J. Org. Chem.* **2005**, *70*, 10524. (b) Gomez, D. E.; Fabbrizzi, L.; Liccheli, M. *J. Org. Chem.* **2005**, *70*, 5717. (c) Gronert, S. *J. Am. Chem. Soc.* **1993**, *115*, 10258.

(61) (a) Amendola, V.; Esteban-Gömez, D.; Fabbrizzi, L.; Licchelli, M. *Acc. Chem. Res.* **2006**, *39*, 343. (b) Boiocchi, M.; Boca, L. D.; Gomez, D. E.; Fabbrizzi, L; Licchelli, M.; Monzani, E. *Chem.—Eur. J.* **2005**, *11*, 3097. (c) Amendola, V.; Boiocchi, M.; Fabbrizzi, L.; Palchetti, A. *Chem.—Eur. J.* **2005**, *11*, 5648. (d) Peng, X.; Wu, Y.; Fan, J.; Tian, M.; Han, K. *J. Org. Chem.* **2005**, *70*, 10524. (e) Gunnlaugasson, T.; Kruger, P. E.; Jensen, P.; Tierney, J.; Ali, H. D. P.; Hussey, G. M. *J. Org. Chem.* **2005**, *70*, 10875. (f) Amendola, V.; Boiocchi, D.; Colasson, B.; Fabbrizzi, L. *Inorg. Chem.* **2006**, *45*, 6138.

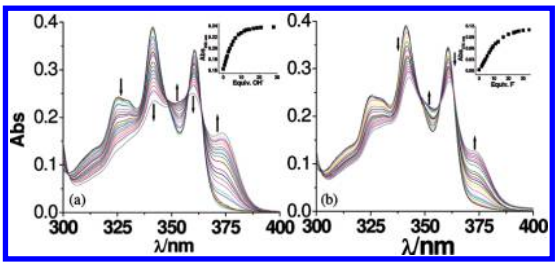

Figure 9. Changes of the UV−vis spectra of H_3Imbzim in CH_3CN/DMF (9:1) upon the addition of (a) OH^- and (b) F^-. The inset shows the absorbance change as a function of the equivalents of OH^- (a) and F^- (b) added.

have close resemblance to the spectra of the receptor with F^- and, to a lesser extent. with AcO^- but not with $H_2PO_4^-$. The result indicates that initially the central imidazole NH (probably most acidic) gets involved through hydrogen-bonding interaction, followed by deprotonation with a huge excess of the anions. It may be noted that the binding constants of the metal complexes with the anions are substantially enhanced (2 orders of magnitude) relative to the ligand H_3Imbzim itself. We believe this to be caused by the Ru^{II} center(s), which makes the bis(benzimidazole) ligand electron-deficient, thereby rendering the imidazole NH protons more available for hydrogen bonding to the anions.

Luminescence Spectra. The complexes **1** and **2**, upon excitation at the wavelengths where their two MLCT absorption maxima are observed, exhibit broad luminescent maxima at 660 nm for **1** and at 685 nm for **2** in CH_3CN at room temperature, which remain unchanged with the energy of excitation wavelengths. The bands have the characteristics of emission from the ^{3}MLCT excited state, which corresponds to a spin-forbidden Ru → bpy transition.[62,63] In solution, at room temperature, the complexes are weak emitters {quantum yields (Φ) = 0.014 for **1** and 0.0013 for **2**} with lifetime $\tau = 175 \pm 10$ ns for **1** (Figure S9 in the Supporting Information) and $\tau = 150 \pm 10$ ns for **2**. The free ligand, H_3Imbzim on excitation at 360 nm fluoresce strongly ($\Phi = 0.5$) at 465 nm in DMF-CH_3CN (1:9) with lifetime of 2.9 ± 0.1 ns (Figure S10).

The sensing of the receptors **1** and **2** for anions was also studied through emission spectral changes in CH_3CN solutions. As can be seen from Figure 10, the original emission bands at 660 nm for **1** and at 685 nm for **2** were almost unchanged upon the addition of Cl^-, Br^-, I^-, NO_3^-, and ClO_4^- anions to a 1.5×10^{-5} M solution of **1** and **2** because of the weaker interaction between them in solution. Upon the addition of an excess of $H_2PO_4^-$, AcO^-, and F^- (up to 8 equiv), the emissions for both **1** and **2** were completely quenched except with $H_2PO_4^-$. In the case of **2**, the addition of 1 equiv each of F^- and AcO^- leads to complete quenching of the emission with consequent red shifts of emission maxima from 685 to 735 nm. Compounds **1** and **2** clearly possess the strongest affinity for F^- and AcO^- and, to a lesser extent, for $H_2PO_4^-$. These

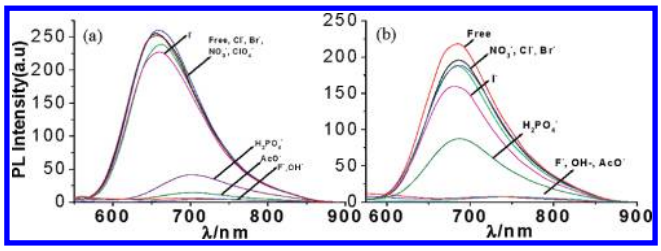

Figure 10. Luminescence spectra of receptors **1** (a) and **2** (b) in CH_3CN solutions in the absence and presence of different anions.

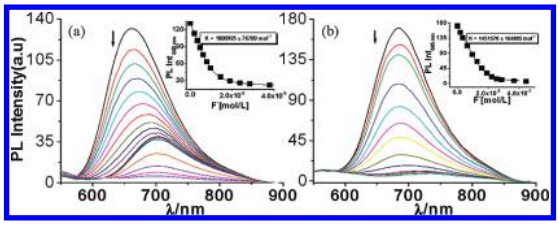

Figure 11. Changes of the photoluminescence intensity of the sensors **1** (a) and **2** (b) in CH_3CN upon the addition of F^-. The inset shows the fit of the experimental emission data to a 1:1 binding profile.

observations are consistent with those of the absorption experiments.

Like absorption, the emission titration experiments also provide quantitative insights into receptor−anion binding. In the luminescence titration experiments, the excitation wavelengths correspond to the isosbestic point found at 485 nm for **1** (Figure 6) and 495 nm for **2** (Figure 7). The lowest-energy emission maxima in both compounds get gradually red-shifted with consequent quenching with increasing anion concentration, indicating a lowering in energy of the excited state and an enhancement of the nonradiative decay.[64] Typically, Figure 11 presents quenching of the steady-state photoluminescence spectra of **1** and **2** measured throughout the fluoride titration.

Upon the addition of 1 equiv each of $H_2PO_4^-$, F^-, and AcO^- to a solution of **1**, the emission maxima red-shifted to 700 nm with significant quenching of the emission intensity. Upon the addition of a large excess of anions (up to 8 equiv), the emission of **1** was completely quenched with both AcO^- and F^- but not with $H_2PO_4^-$ (Figure 11a). By contrast, the addition of only 1 equiv each of AcO^- and F^- to a solution of **2** completely quenched the emission intensity (Figure 11b). The inset to Figure 11 shows the fit of the experimental emission data to a 1:1 binding profile. Table 3 also summarizes all of the emission-data-derived binding constants measured for the sensors toward different anions. Spectrofluorometric titrations of **1** and **2** were also carried out with a standard solution of $[nBu_4N]OH$ (Figures S11 and S12 in the Supporting Information). The monodeprotonated (1 equiv of OH^-) spectral patterns for **1** have close resemblance to the spectra of the receptor in the presence of ca. 1 equiv each of F^-, AcO^-, and $H_2PO_4^-$. Again, like F^- and AcO^-, the bideprotonated form of **1**, $[(bpy)_2Ru(HImbzim)]$, can be achieved through the addition of a large excess of OH^-. In the case of **2**, total quenching of the emission occurred with 1 equiv of OH^- only, as with

(62) Juris, A.; Balzani, V.; Barigelletti, F.; Campagna, S.; Belser, P.; von Zelewsky, A. *Coord. Chem. Rev.* **1988**, *84*, 85.
(63) Kalyanasundaram, K. *Photochemistry of Polypyridine and Porphyrin Complexes*; Academic Press: London, 1992.
(64) Sun, S.-S.; Lees, A. J. *Chem. Commun.* **2000**, 1687.

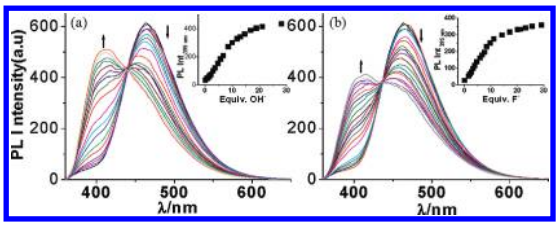

Figure 12. Changes of the photoluminescence intensity of H_3Imbzim in CH_3CN/DMF (9:1) upon the addition of (a) OH^- and (b) F^-. The inset shows the photoluminescence intensity change as a function of the equivalents of OH^- (a) and F^- (b) added.

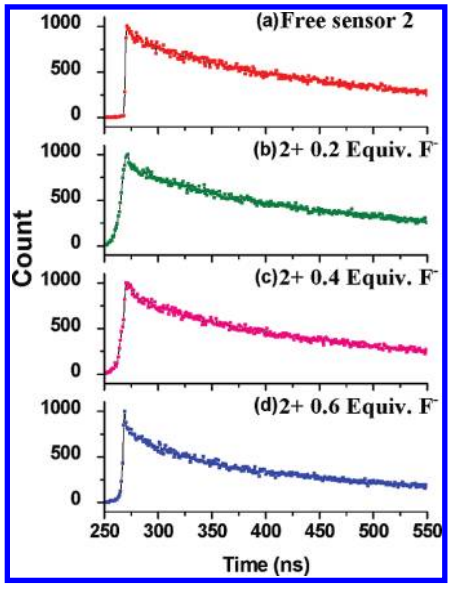

Figure 13. Changes in the time-resolved photoluminescence decay of sensor **2** in CH_3CN at room temperature upon the addition of F^-, obtained with 440 nm excitation. The emission at 685 nm was monitored as a function of time.

AcO^- or F^-. It is evident that the stronger bases and hydrogen-bonding acceptors such as AcO^- and F^- as well as OH^- completely quench fluorescence of the metalloreceptors, implying that the NH protons of coordinated H_3Imbzim/H_2Imbzim$^-$ are trapped by these anions. An almost complete quenching of the emission intensity by F^- and AcO^- over other anion makes **1** and **2** selective fluorescent sensors. Figure 12 presents the changes in the emission spectrum of H_3Imbzim as a function of F^- and OH^-.

As can be seen, the emission peak at 465 nm decreased and a new peak at 415 nm appeared with a clean isoemissive point at 435 nm after the addition of a large excess of F^- and OH^-. With AcO^-, the corresponding change is less, while there is almost no change in the emission spectral profile with other anions.

The luminescence lifetime quenching of **2** as a function of the fluoride concentration is represented in Figure 13. In the absence of fluoride, **2** exhibited a single-exponential lifetime ($\tau = 150 \pm 10$ ns) in acetonitrile at room temperature. During the first two fluoride additions, the intensity decays could be adequately fit to a single-exponential model; however, the lifetime shortened to 80 ± 10 ns (0.2 and 0.4 equiv of F^-). At higher F^- concentrations (0.6 and 1.0 equiv), the intensity decays exhibited complex kinetics that adequately fit a sum of two exponentials. Both exponential components

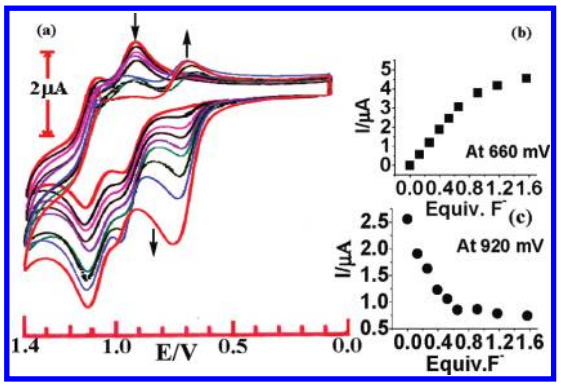

Figure 14. (a) Changes of CVs upon the addition of TBAF to a CH_3CN solution (1.0×10^{-3} M) of **2**. (b) Increase in the current intensity at $E = 660$ mV corresponding to **2** bound with the F^- ion. (c) Decrease in the current intensity at $E = 920$ mV corresponding to $E_{1/2}{}^1$ of free **2** as a function of the equivalents of F^- ion added.

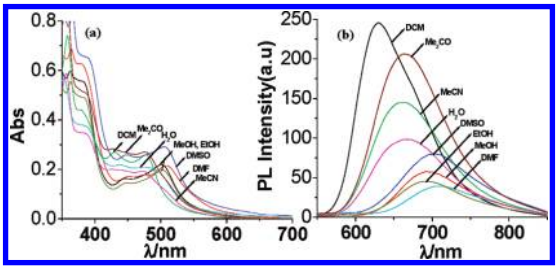

Figure 15. (a) UV−vis and (b) photoluminescence spectra of receptor **1** in different solvents.

remained effectively constant, ranging from 75 to 100 ns (long τ) and from 15 to 20 ns (short τ). These data suggest that there are at least two distinct luminescent species, consisting of anion-bound **2**, whose lifetime is shorter, and free **2**, the sum of which results in the observed lifetime quenching in Figure 13.[30] Thus, the anion-induced lifetime shortening makes complex **2** a suitable lifetime-based sensor for anions.

Redox Activities. CV and OSWV were also used to probe the changes in the redox potentials of the receptors **1** and **2** upon complexation with the anions. The monometallic complex **1** displays a one-electron reversible oxidation wave at 1.08 V due to Ru^{II}/Ru^{III}, while the bimetallic complex **2** shows two successive one-electron reversible oxidation waves due to $Ru^{II}Ru^{II}/Ru^{II}Ru^{III}$ ($E_{1/2}{}^1$) and $Ru^{II}Ru^{III}/Ru^{III}Ru^{III}$ ($E_{1/2}{}^2$) at 0.92 and 1.11 V, respectively, in CH_3CN (vs Ag/AgCl) at 298 K. The electrochemical responses of the sensors in the potential window of 0 to −2.2 V have also been observed with a glassy carbon working electrode. Complex **1** is found to undergo two successive one-electron reversible reductions at −1.45 and −1.77 V, while for complex **2**, the corresponding reduction processes observed at −1.47 and −1.73 V are two-electron processes (Figure S13 in the Supporting Information). From both the cyclic and Osteryoung square-wave voltammograms, it is seen that the current heights of the two reduction waves are almost double compared to that of the individual oxidation waves. The two separated oxidation waves of the dinuclear complex **2** may be due to electronic interactions between the two metal centers because the distance between the two metal centers is relatively small,

Table 4. Absorption and Emission Spectral Data of MLCT Transitions for the Receptors **1** and **2** in Various Solvents

	1		**2**	
solvent	λ_{max}, nm (ε, M^{-1} cm^{-1})	λ_{emi}, nm (Φ)	λ_{max}, nm (ε, M^{-1} cm^{-1})	λ_{emi}, nm (Φ)
DCM	477 (11 670) 430 (12 120)	630 (3.7×10^{-2})	489 (28 970) 450 (30 740)	632 (4.5×10^{-2})
MeOH	500 (11 590) 446 (8620)	695 (4.5×10^{-3})	498 (19 630) 455 (18 240)	720 (9.8×10^{-4})
Me_2CO	476 (11 070) 427 (11 560)	665 (1.7×10^{-2})	493 (24 480) 450 (25 040)	689 (5.5×10^{-3})
EtOH	502 (9800) 449 (7250)	692 (4.5×10^{-3})	500 (22 000) 458 (20 080)	700 (1.3×10^{-3})
MeCN	475 (9230) 425 (10 070)	660 (1.2×10^{-2})	488 (12 500) 447 (13 300)	685 (3.0×10^{-3})
DMF	509 (10 190) 475 (8480)	710 (3.4×10^{-3})	502 (20 490) 475 (19 020)	720 (1.1×10^{-3})
DMSO	505 (12 490) 448 (11 070)	705 (6.6×10^{-3})	500 (20 060) 455 (19 240)	720 (1.4×10^{-3})
H_2O	474 (8530) 437 (8890)	668 (9.1×10^{-3})	484 (21 230) 448 (23 850)	682 (6.1×10^{-3})

viz., 6.124 Å. The wave splitting upon reduction is much smaller (actually the reduction process is a bielectronic process) than that observed upon oxidation because the two bpy centers involved in the reduction are more separated (the centroid-to-centroid distance among the two bpy centers attached to different metal centers extends up to 12.9 Å). The observed behavior is quite similar to that reported for ruthenium(II) complexes of other anionic electron-rich bridging ligands.[29c−h]

The progressive addition of F^-, AcO^-, and $H_2PO_4^-$ ions to a solution of **1** and **2** resulted in a negative shift of the oxidation potentials. It should be noted (Figures S14−S16 in the Supporting Information) that the current intensity associated with the new oxidation peak at 0.84 V due to the anion-bound **1** gradually increases and reaches a limit (ΔE = 0.24 V) when approximately 1 stoichiometric equiv of F^-, AcO^-, and $H_2PO_4^-$ ions is added to the receptor, keeping the $E_{1/2}$ value at 1.08 V for free **1** constant. Upon the addition of a further excess of anions to the solution of **1**, the oxidation peak at 0.84 V continued to shift in the lower potential region up to 0.64 V except with $H_2PO_4^-$. For the bimetallic complex **2**, it is seen from Figure 14 that the current intensity associated with oxidation at 0.92 V corresponding to ${E_{1/2}}^1$ of free **2** gradually decreases, whereas the intensity associated with the new oxidation at 0.66 V gradually increases and reaches a limit when approximately 1 equiv each of F^- and AcO^- ions is added to the receptor. The addition of a large excess of both anions to the solution of **2** causes no further change in the cyclic voltammogram.

The results presented here provide a hint that complexes **1** and **2** could prove useful in the fabrication of electrochemical sensors. The present results also provide support for the notion that modification of the electronic features of benzimidazole through metal complexation might allow for a convenient and general approach to enhancing the anion affinities and possibly modulating the selectivites of benzimidazole-type anion receptors.

For the bimetallic complex **2**, the equilibrium constant K_c for the comproportionation reaction $Ru^{II}Ru^{II}$ + $Ru^{III}Ru^{III}$ ⇌ $2Ru^{II}Ru^{III}$ is obtained from the relation $K_c = \exp(nF\Delta {E_{1/2}}^{ox}/RT)$. The value of K_c, 1.6×10^3 at 298 K, gives a measure of the stability of the mixed-valence species over the homovalent species. By comparison, the value of K_c for an anion-induced deprotonated complex (1.3×10^7) is 4 orders of magnitude greater. This indicates that the mixed-valence state becomes relatively more stabilized when the bridging ligand is deprotonated. The magnitude of K_c depends, inter alia, on the electrostatic and magnetic superexchange interactions and electron delocalization.[65−67] The effect of anion-induced deprotonation in the present case seems to augment electron delocalization in the system.

Solvent Effect. One of the most important aspects of this study is that, in competitive hydrogen-bonding solvents such as CH_3OH, C_2H_5OH, DMF, and DMSO, the color of the complexes changes as compared to those observed in CH_3CN. Figure 15a shows that the positions of the MLCT absorptions are strongly affected by solvents. From Table 4, it is seen that the band maxima shift to longer wavelength with an increase in polarity as well as with the extent of the hydrogen-bonding ability of the solvent. For instance, the lowest-energy MLCT maximum in **1** shifted from 475 nm in CH_3CN to 505 nm in DMSO ($\Delta\lambda_{max}$ = 30 nm; ΔE = 1250 cm^{-1}) with a concomitant change of color from yellow-orange to orange-brown. For **2**, the corresponding change is 606 cm^{-1} (490−505 nm; Figure S18 in the Supporting Information), with the color changing from yellow to orange-yellow.

Figure 15b shows the emission spectra of **1** in different solvents. As compared with the absorption spectra, its emission spectral behavior shows significantly larger solvatochromism. When the solvents are changed, the lowest-energy emission maxima get red-shifted from 630 (CH_2Cl_2) to 705 nm (DMF) (ΔE = 1690 cm^{-1}). In the case of **2**, the corresponding change of the emission maxima is 1081 cm^{-1} (668−720 nm) (Figure S19 in the Supporting Information). It may be noted that in both compounds the emission intensity is quenched to a significant extent with DMF, DMSO, MeOH, and EtOH solvents, indicating a strong hydrogen-bonding interaction with the solvents.

(65) Richardson, D. E.; Taube, H. *Coord. Chem. Rev.* **1984**, *60*, 107.
(66) Crutchley, R. J. *Adv. Inorg. Chem.* **1994**, *41*, 273.
(67) Robin, M. B.; Day, P. *Adv. Inorg. Chem. Radiochem.* **1967**, *10*, 247.

In binary solvent systems, the incremental addition of a high polar solvent to solutions of the complexes in a lower polarity solvent causes a large red shift in both the absorption and emission spectra. For example, when CH_3OH was added gradually to a CH_2Cl_2 solution of **1**, the two MLCT peaks at 478 and 430 nm in successive absorption curves undergo gradual red shifts, during which they pass through two isosbestic points at 493 and 396 nm and are finally shifted to 505 and 448 nm (Figure S20 in the Supporting Information), respectively. With an increase of the ratio of CH_3OH/CH_2Cl_2, the emission maxima of **1** also shifted steadily from 630 to 695 nm with almost a 10-fold decrease in the intensity (Figure S20 in the Supporting Information). The close resemblance of spectra (both absorption and emission) of the receptors in the presence of 1 equiv each of F^-, AcO^-, and $H_2PO_4^-$ to those of the spectra obtained in DMF, DMSO, and MeOH suggests that the first change is a consequence of the formation of an initial hydrogen bonding between the NH protons of the coordinated H_3Imbzim and the corresponding anions, followed by proton transfer.

Conclusion

In conclusion, we have developed new sensors based on the ruthenium(II) bipyridine moiety as a chromophore and the H_3Imbzim ligand as an anion receptor site that can act as colorimetric sensors for F^- and AcO^- and, to some extent, for $H_2PO_4^-$ in solution. The binding properties were also confirmed by absorption, emission, and ^{1}H NMR spectroscopic techniques and by CV. From binding studies, it may be concluded that, at relatively lower concentration, a 1:1 hydrogen-bonded adduct between the metalloreceptors and the anions is formed. However, in the presence of excess of anions, stepwise deprotonation of the two benzimidazole NH fragments occurs, an event that is signaled by the development of intense and beautiful colors visible with the naked eye. Less basic anions (AcO^- and $H_2PO_4^-$) in some cases induce deprotonation of only one NH. Time-resolved photoluminescence decays were also measured for **2** to test its viability as a lifetime-based sensor for anions. It may be possible to conceive the use of these multichannel metalloreceptors in various sensing applications as well as in other situations, such as anion transport and purification, where the availability of cheap and easy-to-make anion receptors would be advantageous.

Acknowledgment. Financial assistance received from the Department of Science and Technology, New Delhi, India (Grant SR/S1/IC-06/2006), and the Council of Scientific and Industrial Research, New Delhi, India [Grant 01(2084)/06/EMR-II], is gratefully acknowledged. Thanks are due to the Department of Inorganic Chemistry of Indian Association for the Cultivation of Science, Kolkata, India, for single-crystal X-ray data. D.S., S.D., and C.B. thank CSIR for their fellowship.

Supporting Information Available: X-ray crystallographic file in CIF format for compounds **1** (CCDC 753394) and **2** (CCDC 743288), Tables S1 and S2, and Figures S1−S20. This material is available free of charge via the Internet at http://pubs.acs.org. The atomic coordinates for these structures have been deposited with the Cambridge Crystallographic Data Centre. The coordinates can be obtained, upon request, from the Director, Cambridge Crystallographic Data Centre, 12 Union Road, Cambridge CB2 1EZ, U.K.